

Aberystwyth University

Infrared radiofluorescence (IR-RF) dating

Murari, Madhav Krishna; Kreutzer, Sebastian; King, Georgina; Frouin, Marine; Tsukamoto, Sumiko; Schmidt, Christoph; Lauer, Tobias; Klasen, Nicole; Richter, Daniel; Friedrich, Johannes; Mercier, Norbert; Fuchs, Markus

Published in:

Quaternary Geochronology

DOI:

[10.1016/j.quageo.2021.101155](https://doi.org/10.1016/j.quageo.2021.101155)

Publication date:

2021

Citation for published version (APA):

Murari, M. K., Kreutzer, S., King, G., Frouin, M., Tsukamoto, S., Schmidt, C., Lauer, T., Klasen, N., Richter, D., Friedrich, J., Mercier, N., & Fuchs, M. (2021). Infrared radiofluorescence (IR-RF) dating: A review. *Quaternary Geochronology*, 64, Article 101155. <https://doi.org/10.1016/j.quageo.2021.101155>

Document License

CC BY-NC-ND

General rights

Copyright and moral rights for the publications made accessible in the Aberystwyth Research Portal (the Institutional Repository) are retained by the authors and/or other copyright owners and it is a condition of accessing publications that users recognise and abide by the legal requirements associated with these rights.

- Users may download and print one copy of any publication from the Aberystwyth Research Portal for the purpose of private study or research.
- You may not further distribute the material or use it for any profit-making activity or commercial gain
- You may freely distribute the URL identifying the publication in the Aberystwyth Research Portal

Take down policy

If you believe that this document breaches copyright please contact us providing details, and we will remove access to the work immediately and investigate your claim.

tel: +44 1970 62 2400

email: is@aber.ac.uk

Infrared Radiofluorescence (IR-RF) dating: a review

Madhav Krishna Murari^{1,2}, Sebastian Kreutzer^{3,4,*}, Georgina King⁵, Marine Frouin^{6,7}, Sumiko Tsukamoto⁸, Christoph Schmidt^{5,9}, Tobias Lauer¹⁰, Nicole Klasen¹¹, Daniel Richter^{10,12}, Johannes Friedrich⁹, Norbert Mercier⁴, Markus Fuchs¹

¹Department of Geography, Justus Liebig University, Giessen, Germany

²Geochronology Project, Inter-University Accelerator Centre, New Delhi, India

³Geography and Earth Sciences, Aberystwyth University, Aberystwyth, United Kingdom

⁴IRAMAT-CRP2A, UMR 5060, CNRS - Université Bordeaux Montaigne, Pessac, France

⁵Institute of Earth Surface Dynamics, Université de Lausanne, Lausanne, Switzerland

⁶Department of Geosciences, Stony Brook University, Stony Brook, NY, United States

⁷Research Laboratory for Archaeology and the History of Art, School of Archaeology, Oxford University, Oxford, United Kingdom

⁸Leibniz Institute for Applied Geophysics, Hannover, Germany

⁹Chair of Geomorphology, University of Bayreuth, Bayreuth, Germany

¹⁰Department of Human Evolution, Max Planck Institute for Evolutionary Anthropology, Leipzig, Germany

¹¹Institute of Geography, University of Cologne, Cologne, Germany

¹²Freiberg Instruments GmbH, Freiberg, Germany

***corresponding author:** sebastian.kreutzer@aber.ac.uk

Abstract

Luminescence dating methods on natural minerals such as quartz and feldspars are indispensable for establishing chronologies in Quaternary Science. Commonly applied sediment dating methods are optically stimulated luminescence (OSL) and infrared stimulated luminescence (IRSL). In 1999, Trautmann et al. (1999a, b) proposed a new related technique called infrared radiofluorescence (IR-RF). IR-RF denotes the infrared luminescence signal resulting from exposure to ionizing radiation and potentially offers a significant methodological advance compared to OSL and IRSL regarding luminescence signal stability, dating range and required measurement time. The method has rarely been applied due to a lack of commercially available measurement equipment but experienced a revival during the last years. The present article provides a state-of-the-art overview of the physical background of IR-RF, its challenges, applications and the potential as a dating method. The paper particularly addresses practical considerations for applying IR-RF dating, including signal bleachability and saturation behaviour, and summarizes proposed solutions.

Keywords: Infrared radiofluorescence; Radioluminescence; Feldspar; Chronology; Luminescence dating

1 Introduction

In the late 1990s, Trautmann et al. (1998) characterized radioluminescence signals, the emission stimulated by ionizing radiation, from various feldspar specimens to investigate their potential for dating applications. Focusing first on radiation-induced emissions in the UV and yellow wavelength range, where luminescence signal increases with radiation dose, they incidentally observed the opposite for potassium bearing (K-) feldspar specimen such as microcline and orthoclase: a dose-dependent signal decrease of the emission centred at 854 nm (1.45 eV; based on peak tail fitting only). Later, Trautmann et al. (1999a, b), Schilles (2002) and Erfurt and Krbetschek (2003a) determined that the emission peak was centred at 865 nm (1.43 eV). Trautmann et al. (1998) recognized that this emission energy is similar to the excitation energy used for infrared stimulated luminescence (IRSL, Hütt et al., 1988) and consequently interpreted this process as a luminescent transition (trapping) of electrons. Their pioneer work paved the way to what is known today as infrared radiofluorescence (IR-RF) dating; the method first proposed by Trautmann et al. (1999a, b) and termed by Erfurt and Krbetschek (2003a, b). The IR-RF signal is believed to be a direct measure of the fraction of empty electron traps, unlike conventional luminescence dating methods such as those based on thermoluminescence (TL, cf. Aitken, 1985a), optically stimulated luminescence (OSL, Huntley et al., 1985; Aitken, 1998) and infrared stimulated luminescence (IRSL, Hütt et al., 1988), for which the signals are associated with more complex recombination pathways. Since the IR-RF signal intensity *decreases* with increasing dose, it can be used for dosimetry and dating purposes. IR-RF may provide advantages over conventional single aliquot regenerative (SAR, Murray and Wintle, 2000) dose, IRSL dating methods (e.g., SAR IRSL, Wallinga et al., 2000) or its derivatives deploying higher reading temperatures (post-IR IRSL, Thomsen et al., 2008; MET-pIRIR, Li and Li, 2011a) in terms of required measurement time (relatively short protocol, cf. Erfurt and Krbetschek, 2003b), resolution of the dose-response curve (continuous recording of data points) and dating range (Sec. 7). Nevertheless, IR-RF as a dating method is still subject to ongoing research, with its general applicability being questioned (Buylaert et al., 2012). On the contrary, recent technological and methodological work, e.g., on the optical resetting of the IR-RF signal, and improved routines for dose estimation have yielded promising results (Frouin, 2014; Frouin et al., 2015, 2017; Huot et al., 2015; Kreutzer et al., 2017; Murari et al., 2018).

This contribution provides an overview of past and recent developments of IR-RF from K-feldspar as a dating method. We summarize current knowledge on existing models on the origin of IR-RF, outline commonly applied measurement procedures and equipment, and highlight shortfalls, challenges and open questions. Understanding what remains unknown may stimulate discussions and lead to improved experimental designs towards a full establishment of IR-RF as a valuable chronological tool.

2 Origin of the IR-RF signal and relevant models

The 1.43 eV (865 nm) IR-RF emission of K-feldspar (Trautmann et al., 1999a, b; 1.45 eV in Trautmann et al., 1998, see below for an explanation) has the same energy as the typical excitation maximum of IRSL (Hütt et al., 1988; Poolton et al. 2002a, b), which led Trautmann et al. (1998) to suggest that both signals are derived from the same principal electron trap. More recent observations of infrared photoluminescence (IR-PL; Prasad et al., 2017) seem to support this hypothesis (see also Kumar et al., 2018). Further studies by Kumar et al. (2020) generally confirmed this view but extended the understanding by assigning two different defect sites to the principal trap based on their cathodoluminescence measurements.

Trautmann et al. (1999a, b) and Trautmann (2000) proposed a model for the IR-RF emission of feldspar whereby IR-RF results from the transition of an electron from the conduction band to the ground state of the IRSL trap through the excited state.

Figure 1 illustrates the different electronic transitions associated with IRSL and IR-RF production in one plot. Please note: Although we compiled different ideas in one figure, our graphical representation *should not* be considered a new model. In Fig. 1, continuous exposure to ionizing radiation leads to a constant flow of electrons from the valence band to the conduction band [a], from which electrons can either recombine radiatively [b] or non-radiatively (not shown for clarity), or become trapped [c]. As irradiation persists, the IRSL trap [c] becomes filled, resulting in more electrons recombining radiatively [b], accounting for the observed rise in the ultraviolet (UV)-RF and visible light (VIS)-RF emissions at higher doses (Trautmann et al., 1999a). However, this model raises two major questions: (1) why does the IR-RF signal not fully saturate during laboratory irradiation, resulting in a zero or negligible IR-RF signal, and (2) to bleach, why does the IR-RF signal require exposure to light of higher energies than IR (e.g., Trautmann et al., 1998,

1999a, b; Frouin et al., 2015, 2017), whereas the IRSL signal from the same trap could be efficiently reset through exposure to infrared light?

Figure 1

(Models)

To explain why the IR-RF signal does not appear to saturate, Trautmann et al. (1999a) first considered electron release throughout irradiation due to the low thermal stability of the IRSL trap, resulting in the replenishment of free electron-hole pairs and thus a continuously decaying IR-RF signal. However, this hypothesis contradicts a measured lifetime of the IRSL trap in the range of Ga (Murray et al., 2009). An alternative explanation not considered by Trautmann et al. (1999a) is the loss of trapped electrons by athermal tunnelling, known as anomalous fading of feldspar (e.g., Wintle 1973; Spooner 1992; Visocekas, 1993; Huntley and Lian, 2006) and more specifically, the anomalous fading of the IRSL feldspar trap (e.g., Spooner 1992; Huntley and Lamothe, 2001) (transition [d] in Fig. 1), which we summarised in Sec. 5.6. Instead, Trautmann et al. (1999a) preferred a model already suggested by Schön et al. (1942) and Klasens (1946) for sulphide phosphors, with a proposed transfer of holes from the valence band to the IRSL trap throughout irradiation, effectively increasing the defects trapping capacity (transition [e] in Fig. 1).

To address the different bleaching behaviour of IR-RF and IRSL signals, Trautmann et al. (2000a) modified their earlier model, relating the bleaching of the IRSL signal to localized electron transitions after the suggestion by Poolton et al. (1995). Following IR exposure, an electron is only excited to the excited state of the trap ([f] in Fig. 1), which is paired with the excited state of a neighbouring recombination centre, allowing a localized transition. Thus, the IRSL emission would relate to the radiative relaxation of the electron to the ground state of the recombination centre. Trautmann (2000) and Trautmann et al. (2000a) determined from pulse-annealing experiments that bleaching of the IRSL trap is limited by the number of available recombination centres, suggesting thermal instability of trapped electrons could reduce the density of holes. They drew this conclusion from the IR-RF signal's stability up to temperatures of 400 °C, whereas IRSL and the related VIS-RF signals depleted at temperatures >300 °C. Trautmann (2000) and Trautmann et al. (2000a) concluded that the IRSL electron-hole population accounts for only ~1.5

% of the total potential IRSL trap occupancy, implying that most of these trapped electrons do not have the possibility of recombining with a hole during IR stimulation. A phenomenon that Trautmann (2000) and Trautmann et al. (2000a) did not consider, and which may influence these effects to some extent, is athermal signal loss (i.e., anomalous fading). Following the model of Huntley (2006), ground state tunnelling [d in Fig. 1] would result in preferential recombination of unstable charge with proximal recombination centres, which may otherwise have been involved in localized transitions from the IRSL trap. Athermal de-trapping results in a non-linear increase of IRSL with dose, an effect recorded and highlighted by Trautmann (2000) and Trautmann et al. (2000a).

2.1 Defects related to IR-RF and IRSL

The exact identification of defects responsible for electron and hole trapping in feldspar is subject to ongoing research, and as such, the physical nature of the IRSL and IR-RF trap remains under debate. The traps and recombination centres of K-feldspars have mainly been assigned based on indirect measurements and correlation studies (e.g., Baril and Huntley, 2003a; Erfurt 2003a, b; Erfurt and Krbetschek, 2003b). Krbetschek et al. (1997) discussed the principal K-feldspar luminescence emissions and their possible origins for different excitation methods. The most common emission bands for K-feldspar are listed in Table 1 (please also note the references given therein).

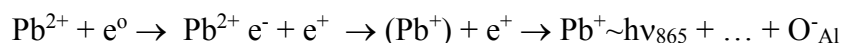
Table 1

(Traps and recombination centres)

It appears that in the literature Fe^{3+} and Pb^{2+} ions have been identified as the main centres which are believed to be responsible for the presence of the red to deep-red emission (~ 1.7 eV; Prasad and Jain, 2018) in feldspar. Kumar et al. (2018) tried to correlate their IR-PL findings (Prasad et al., 2017) with the IR-RF signal. Their work suggested that the same defect participated in the production of IR-RF and IR-PL. However, they speculated that IR-PL, contrary to IR-RF, is “site-selective”, i.e. IR-PL preferentially probes centres leading to the emission at ca 1.30 eV (955 nm) whereas the IR-RF emission may be ‘contaminated’ by emissions from other centres, such as Fe^{3+} , related to the emission band near 680 nm to 740 nm (e.g., Geake et al., 1977; Telfer and Walker, 1975; White et al., 1986; Brooks et al., 2002; Finch and Klein, 1999; Krbetschek et al., 2002;

Prasad and Jain, 2018). Most recent work by Kumar et al. (2020), reporting infrared cathodoluminescence (IRCL) experiments at 7 K, give evidence for a correlation of emission peak position and K-concentration. They further propose Fe^{4+} as a defect competing for electrons with the principal trap. Furthermore, the red emission's peak location has been observed to be related to the composition of feldspar samples (e.g., Finch and Klein, 1999; Krbetschek et al., 2002). In contrast, the Pb^{+} centre appears to be related to the IR-RF emission bands between ca. 860 nm and 910 nm (e.g., Nagli and Dyachenko, 1988; Erfurt 2003a, b; Erfurt and Krbetschek, 2003a).

Erfurt (2003a) and Erfurt and Krbetschek (2003a) observed an increase of IR-RF signal intensity with increasing Pb content for concentrations on the order of 30 ppm to 1,400 ppm, and proposed that the IR-RF emission may be associated with the excitation of Pb^{2+} to monovalent $(\text{Pb}^{+})^*$ which subsequently relaxes to the ground state of Pb^{+} , emitting photons at 1.43 eV. Schematically it reads (adapted from Ostrooumov 2016, p. 152 for amazonite):



However, this hypothesis remains unproven, and earlier electron paramagnetic resonance (EPR) studies have indicated that Pb^{+} is only found in amazonite, a specific type of microcline where Pb^{+} occupies a K^{+} position (Marfunin and Bershov, 1970; Marfunin, 1979). In contrast, Poolton et al. (2002b) hypothesised that the IRSL trap is a simple hydrogenic defect, calculating an optical transition at 1.48 ± 0.04 eV, close to that observed in the K-Na feldspar series.

2.2 IR-RF model and related phenomena

Since Trautmann et al. (1998, 1999a, 2000a) proposed a model to explain the processes of (IR)-RF of feldspar, our understanding of luminescence processes in feldspar has improved considerably, driven mainly by the developments around conventional IRSL (e.g., Wallinga et al., 2000; Huntley and Lamothe, 2001; Lamothe et al., 2003; Auclair et al., 2003; Murray et al., 2009; Kars and Wallinga 2009; Pagonis and Kulp, 2017; Pagonis et al., 2013, 2019; Lamothe et al., 2020), the post-IR IRSL (also pIRIR) measurement protocols (Thomsen et al., 2008; Buylaert et al., 2009), time-resolved IRSL investigations (e.g., Jain and Ankjærgaard, 2011) as well as IR-PL (Prasad, 2017; Prasad et al., 2017, 2018; Kumar et al., 2020).

Figure 1 shows a band-gap diagram which describes models for IRSL, post-IR IRSL and IR-RF. The presence and importance of the sub-conduction band tail-states are now widely recognized (Poolton et al., 2002a, 2009; Jain and Ankjærgaard, 2011) and anomalous fading (athermal signal loss; Wintle, 1973 for TL; Spooner 1992 for stimulation at 514.5 nm and ~880 nm) from the IRSL trap is generally regarded as ubiquitous in feldspar (e.g., Huntley and Lamothe, 2001) (transition [d] in Fig. 1). The largest inconsistency between the IR-RF models and more recent studies is that the former models did not consider the effects of hole distribution (i.e., recombination distance) and anomalous fading.

Excitation spectra of feldspar revealed the characteristic resonance at ~1.4 eV (1.43 eV, Hütt et al., 1988; see also above), which is superimposed on a rising continuum, now recognized as relating to the sub-conduction band-tail states (Poolton et al., 2002a, 2009). IRSL preferentially samples electrons which can recombine with proximal holes, either through tunnelling from the ground state of the IRSL trap (transition [d] in Fig. 1) or via a localized transition (transition [f] in Fig. 1). Higher energy stimulation of the IRSL trap or higher temperature stimulation (phonon-assisted diffusion) allows electrons to recombine via diffusion through the band-tail states (Poolton et al. 2002a; Jain and Ankjærgaard, 2011) (transition [g] in Fig. 1). For post-IR IRSL signals, which are measured at elevated temperatures of typically 225 °C or 290 °C (pIRIR₂₂₅ or pIRIR₂₉₀), this enables more distal recombination centres to be accessed (Jain and Ankjærgaard, 2011), which have greater athermal (Huntley 2006; Jain and Ankjærgaard, 2011) and thermal stability (Thomsen et al., 2010; Li and Li, 2011b, 2013; Fu et al., 2012). However, pIRIR signals are systematically harder to bleach than IRSL signals (e.g., Li and Li, 2011a).

In general, the IR-RF signal is known to bleach less efficiently than the low-temperature IRSL signal with infra-red light (Trautmann, 1999; Trautmann et al., 1999a; Frouin, 2014; Frouin et al., 2015) and recently it has been shown that the bleaching rate is similar to that observed for the pIRIR₂₉₀ signal (Frouin et al., 2017). This comparably slow bleachability agrees with the apparently high thermal stability of the IR-RF signal (at least up to 350 °C, cf. preheat vs curve shape experiments by Erfurt and Krbetschek, 2003b, their Fig. 7). However, further investigations are required to constrain the thermal stability of IR-RF signal and its susceptibility to anomalous fading.

3 Measurement devices

The first IR-RF studies were carried out on home-made systems (Trautmann et al., 1998, 1999a; Schilles and Habermann, 2000; Erfurt et al., 2003), which differ from the ready-to-use systems available today (Lapp et al., 2012; Richter et al., 2013). The device described in Trautmann et al. (1998) was equipped with a spectrometer for K-feldspar IR-RF exploration. However, because the spectrometer was limited to 800 nm (Trautmann et al., 1998, 1999b), first peak investigations were based on signal extrapolation (Trautmann et al., 1998). After identifying the dose-dependent peak (Trautmann et al., 1999a) at 865 nm, the integrated RF signal around this peak was used for RF dose estimation. Schilles and Habermann (2000) and Erfurt (2003b) went one step further and attached a photomultiplier tube with a filter combination optimized to limit the measured luminescence to the 865 nm emission closely. Tables 3 and 4 summarize the details of various instruments concerning signal detection and sample bleaching parameters. Figures 2 A–D provide different technical realizations for measuring the RF signal from K-feldspar samples.

Figure 2 A B C D

(All IR-RF devices)

3.1 Stimulation or irradiation unit

Radiofluorescence (RF) is the light emission caused by ionizing radiation. Therefore, stimulation sources can either be ionizing charged particles (ions, electrons or protons) or high energy photons (X-ray or γ -ray). The custom-made devices were equipped with $^{137}\text{Cs}/^{137}\text{Ba}$ sources ($t_{1/2} \sim 30.08$ a) (Schilles and Habermann, 2000), while other (commercially) available RF equipment has $^{90}\text{Sr}/^{90}\text{Y}$ sources ($t_{1/2} \sim 28.8$ a) (Lapp et al., 2012; Richter et al., 2012, 2013). Details of the radiation sources are provided in Table 2. The major differences between these radiation sources are activity, radiation type and energy spectra. The $^{137}\text{Cs}/^{137}\text{Ba}$ radiation sources in the home-made devices, e.g., used by Trautmann et al. (1999a), Schilles (2002) and Erfurt et al. (2003), emit β -particles and γ -photons with mean energies of 187.1 keV and 662 keV, respectively. At the same time, ^{137}Cs is also a γ -photon emitter, but the IR-RF stimulation by γ -rays was considered being negligible in comparison to the β -particles (Trautmann, 1999, p. 16). The $^{90}\text{Sr}/^{90}\text{Y}$ source emits a broad energy spectrum with mean β -energies around 195.8 keV. Other differences regarding the stimulation

sources are the design and the way of irradiating the sample (planar radiation source geometry vs ring source geometry). The ring source design (Richter et al., 2012) allows the detector to be mounted directly above the source. For the planar sources, the light collection is realized by an optical light guide (Lapp et al., 2012) or using light reflected to the detector (Schilles, 2002). The indirect light collection has the advantage of reducing unwanted signal contributions induced in the detection system due to bremsstrahlung, but it usually comes at the cost of reduced detection efficiency. Additionally, the ring-type sources have been reported as delivering a highly spatially homogenous dose rate (Richter et al., 2012), relative to planar sources. Common to all types of sources and geometries is the underlying assumption of measuring a comparable IR-RF signal.

Table 2

(Irradiation units)

3.2 Detection and filter combination

Initial studies on IR-RF were based on spectrometer measurements to identify IR-RF peaks and characterize their behaviour. Trautmann et al. (1998) identified the presence and behaviour of the IR-RF peak around 854 nm based on curve fitting of a partially measured peak, but later (Trautmann et al., 1999a, b) reassigned the peak position to 865 nm using an improved spectrometer. Erfurt (2003b) and Schilles (2002) studied this peak in detail with a spectrometer and a photomultiplier tube in conjunction with optical filters (Sec. 5.1). The spectrometers' relevant details are provided in Table 3, and Fig. 3 shows the efficiency of different spectrometer systems.

Table 3

(Spectrometer overview)

Figure 3

(Spectrometer transmission)

Table 4 provides detailed detector settings applied to measure the IR-RF signal. The main difference between the devices is the filter combination, and thus the detection window. However, all types of filters centre around 865 nm and the usage of different filters reflects mainly the availability of filters when the equipment was delivered. Trautmann et al. (1999a) recommended centring around 865 nm and avoiding interference from the 710 nm peak. This idea was also

followed by Erfurt and Krbetschek (2003b) using a detection window of 865 ± 20 nm, considering the broadening effect of the 710 nm peak with increasing dose (Sec. 5.1). The devices used by Schilles (2002) and Erfurt (2003b) both had the same type of photomultiplier tube (PMT) (Hamamatsu R943-02) with a quantum efficiency of ~ 5 % at 865 nm. The quantum efficiency of commercial *lexsyg* and *Risø* readers is about ~ 12 % at that wavelength, both employing the same PMT (Hamamatsu H7421-50), but the efficiency drops to 0.001 % for wavelengths > 900 nm. The PMTs of these commercial devices have a lower efficiency for the potentially interfering signals > 900 nm but relatively high efficiency for the 710 nm peak (Erfurt and Krbetschek, 2003b), which might significantly interfere with the main IR-RF peak. The bandpass for different systems used in the past and present are shown in Figs. 4 A and B.

Table 4

(detector settings)

Figure 4 A B

(PMT efficiency and filter combinations)

3.3 Bleaching units

Table 5 summarizes the information on the commonly used bleaching units. In the device used by past researchers (e.g., Schilles and Habermann, 2000; Erfurt et al., 2003) the sample geometry was fixed, i.e., the sample was not moved between different measurement steps. Thus, the IR-RF signal's bleaching was done by connecting a solar lamp using an optical fibre. In this design, IR cut-off filters were used to avoid excess heating due to the high intensity of light of the solar lamp. In contrast, inside commercial devices for IR-RF measurement and bleaching (e.g., *lexsyg* and *Risø*) the sample moves to different positions. The *Risø* system is equipped with powerful UV LEDs (~ 700 mW), and the *lexsyg* device has an inbuilt LED solar simulator that combines up to six wavelengths with the option of varying the power of each LED (Richter et al., 2013; see Table 5).

Table 5

(bleaching units)

3.4 Sample geometry

Krbetschek et al. (2000) and Erfurt and Krbetschek (2003b) recommended a fixed geometry during IR-RF measurements. They observed a high dispersion in IR-RF dose distributions attributed to geometry changes (e.g., grain movements) when samples were bleached outside the reader. Buylaert et al. (2012) did not observe any changes in the IR-RF signal due to the movement of the sample from one position to another (cf. Fig 3b in Buylaert et al., 2012). Similarly, Frouin et al. (2015, 2017) did not report dose dispersions caused by the movement of the sample inside the reader for their measurements using a *lexsyg research* reader. Later, Kreutzer et al. (2017) attributed a large part of the inter-aliquot scatter to unwanted machine-induced geometry changes, which, however, may have affected only their particular reader. Nevertheless, in summary, it appears to be advisable to aim for a stable sample geometry and check the results for unwanted effects, enlarging the D_e distribution (cf. Kreutzer et al., 2017).

4 Sample preparation methods

IR-RF sample preparation methods extract K-feldspar enriched mineral grains following routine procedures (e.g., Preusser et al., 2008). After sieving and chemical treatments with HCl and H₂O₂, density separation using heavy-liquids (e.g., lithium heteropolytungstates or sodium polytungstate) extract feldspar grains. Additional (froth) flotation (e.g., Herber 1969; application examples: Miallier et al., 1983; Sulaymonova et al., 2018) can be applied to enrich the K-feldspar concentration further; a procedure that the Freiberg group has mainly used in the context of IR-RF (e.g., Trautmann, 1999; Erfurt 2003b). Flotation likely provides a better yield in terms of better separation of quartz and feldspar mineral phases. Despite requiring extra laboratory equipment and staff training, flotation has unmined potential for further enriching the K-feldspar fraction (e.g., via selective flotation: Larsen et al., 2019) with possible implications for measured IR-RF signals.

To remove the outer α -irradiation affected layer of coarse K-feldspar grains ($> 90 \mu\text{m}$) a low concentration ($\leq 10 \%$) HF treatment was often used (e.g., Wagner et al., 2010; Lauer et al., 2011). However, the practice of etching of coarse grain K-feldspar was already questioned by Duller (1992), who described non-uniform etching along the lines of weakness within the mineral. Porat et al. (2015) recalled caution if HF is applied to feldspar grains because HF etching might significantly modify the luminescence properties of K-feldspar, and thus Porat et al. (2015) suggest

etching times <15 min. Frouin et al. (2017) reported inconclusive, younger and highly scattered, IR-RF results for two samples (BT714, BT715) after prolonged HF treatment (10 %, 40 min), while this was not observed for another, non-etched, sample from the same site (BT706). Although the systematic effect of HF treatments with different timings and concentration on the IR-RF signal remains unexplored, HF treatment appears to be dispensable.

5 IR-RF signal characteristics

5.1 IR-RF spectroscopy: Signal identification and measurement optimization

The IR-RF signal composition was extensively studied using a home-made spectrometer in combination with a liquid nitrogen-cooled charged coupled device (CCD) detector (Trautmann et al., 1998, 2000b; Krbetschek and Trautmann, 2000). Their spectroscopic investigations of IR-RF from feldspar revealed many peaks centred at various wavelengths. However, the 865 nm emission peak was found to be stable with its intensity decreasing with increasing dose. K-feldspar showed the highest signal intensity at this wavelength compared to other feldspar compositions. Trautmann (1999) and Schilles (2002) noticed that the spectrum of K-feldspar could be fitted with two Gaussian functions centred at 710 nm (1.75 eV) and 865 nm (1.43 eV). Later, Erfurt (2003b) improved the spectrometer used by Trautmann (1999) and recognized that the data required a minimum of three Gaussian functions to fit the emission spectrum, with a third emission centred at ~910 nm (1.35 eV; Erfurt and Krbetschek, 2003a). The spectroscopic study of these peaks provided the appropriate detection range (filter combination) required for isolating the main IR-RF peak at 865 nm from other neighbouring emissions (Krbetschek et al., 2000). A typical raw spectrum for K-feldspar shows many emission peaks (Fig. 5C after Schilles, 2002) and Trautmann et al. (1999a) demonstrated that the peak intensity at 865 nm decreases with increasing dose, whereas the intensity of the 710 nm peak increases with dose. Furthermore, Trautmann et al. (1998) observed that the 710 nm peak is unstable and vanished within a few hours following irradiation. Both the 710 nm and 910 nm¹ emissions may interfere with the main IR-RF peak (865 nm), which filters can minimise. The effect of such a filter can be simulated using three superimposed Gaussian

¹920 nm in Erfurt and Krbetschek (2003b), however, henceforth termed '910 nm' emission.

functions (Fig. 5A and Fig. 5B similar to Erfurt and Krbetschek, 2003b). Table 4 summarizes all devices' filter combinations to isolate the peak centred at a wavelength of 865 nm.

Figure 5 A B C

(IR-RF peaks in feldspar)

5.2 IR-RF signal resetting

The success of (optical) luminescence dating methods relies on resetting the luminescence signal during sediment transport prior to burial. For IR-RF, the signal intensity increases with light exposure after several minutes to several hours and reaches its highest value when all traps are empty. The bleachability of the IR-RF signal was assessed by bleaching until a plateau is formed between the IR-RF signal vs bleaching time. A constant plateau indicates no further signal increase, i.e., the IR-RF signal is at its maximum, and all IR-RF related traps are empty. In the first IR-RF bleaching experiments (Trautmann et al., 1999a), natural direct sunlight (VIS to UV component, Fig. 6A) was used for a few hours (between 2 h and 5 h of daylight exposure in February in Freiberg, Germany) to bleach the IR-RF signal. Later, Trautmann et al. (2000a) showed that wavelengths shorter than 500 nm were more efficient at resetting the IR-RF signal (Fig. 6B) and Krbetschek et al. (2000) demonstrated that only a few minutes (~5–10 min) were required to reset the signal, using a 200 W Hg-lamp (Table 5 for an overview of the settings) along with a heat-absorbing filter (Fig. 6C). Further bleaching experiments were conducted using a 300 W OSRAM 'Ultravitalux' sunlamp placed at a distance of 35 cm from the aliquot for 6.5 h (Krbetschek et al., 2000) or an on-board lamp (250 W OSRAM metal halide), using fibre optics, which delivered ~100 mW cm⁻² to the aliquot for 30 min.

Figure 6 A B C D

(Bleaching)

Buylaert et al. (2012) compared the D_e values of samples with independent age control. They obtained different values between aliquots that were bleached with UV LEDs (delivering 700 mW cm⁻²) with an exposure time of 25 min, compared to bleaching with a Hönle SOL 2 solar simulator for 4 h. Samples bleached with the Hönle SOL2 resulted in older, but partly also more consistent ages compared to the independent age control (cf. Buylaert et al., 2012, their Fig. 7).

Later Varma et al. (2013) concluded that exposure of 800 s is optimal for resetting the IR-RF signal using the aforementioned UV LED (delivering 700 mW cm^{-2}).

Frouin et al. (2015) systematically compared the bleaching behaviour of monochromatic light and a solar simulator spectrum. In their study, they showed that: i) K-feldspars of various origins exhibit the same behaviour during bleaching experiments, and ii) the IR-RF signal can be bleached by all wavelengths, ranging from 365 nm to 850 nm, and iii) the IR-RF signal can be completely reset in nature and cannot be “over-bleached” in the laboratory even with the use of longer time exposures. Finally, they recommend a solar spectrum close to the terrestrial solar spectrum with minimal UV light contribution. They achieved this by individually adjusting the monochromatic LEDs' power in their luminescence reader and stated that this spectrum delivered a sufficient amount of power (375 mW cm^{-2}) to bleach the IR-RF signal in minimum time at ambient temperature (Frouin et al., 2015). Furthermore, they showed that the onset of a bleaching plateau started after 3 h to 4 h of light exposure (cf. Fig. 4 in Frouin et al., 2015). Specifically, within this light spectrum, the power of the UV (325 nm) LED was reduced to 10 mW cm^{-2} as this wavelength is absorbed by the atmosphere and its presence in the terrestrial solar spectrum is minimal. Regardless, this low power, Frouin (2014, her Fig. 28) showed that UV bleaches most efficiently within the first seconds before it reaches a plateau after ca. 40 h. Although an artificial bleaching spectrum using only six wavelengths (LEDs) cannot match the terrestrial solar spectrum, it may remain a good approximation of natural bleaching conditions (typical irradiance on Earth of 90– 100 mW cm^{-2} ; ASTM international, 2012). A comparison between the bleaching behaviour of the IR-RF signal measured at 70°C (Sec. 6.1) with other variants of the IRSL signals of K-feldspar showed that IR-RF seems to bleach at a similar rate to the pIRIR_{290} signal but much slower than the IRSL_{50} signal (Frouin et al., 2017; Fig. 6D). However, a similar bleaching rate compared to the pIRIR_{290} signal does not guarantee a complete reset of either signal (i.e., pIRIR_{290} and IR-RF); various studies have shown that the pIRIR_{290} signal is hard to bleach and can have large residual doses even after 4 h of solar simulator bleaching (e.g., Buylaert et al., 2012; Li et al., 2014). It may take up to ~ 300 h to reach a constant residual dose (Yi et al., 2016). In summary, Frouin et al. (2015) recommended a minimum of 3 h bleaching using the inbuilt solar simulator of their equipment with the following settings: 365 nm (10 mW cm^{-2}), 462 nm (63 mW cm^{-2}), 525 nm (54 mW cm^{-2}), 590 nm (37 mW cm^{-2}), 623 nm (115 mW cm^{-2}), and 850 nm (96 mW cm^{-2}).

5.3 Phosphorescence

In the context of IR-RF, two types of phosphorescence have been observed: (1) Phosphorescence after bleaching (Fig. 7) and (2) phosphorescence after irradiation (so-called radiophosphorescence). *Phosphorescence after bleaching* was considered by Erfurt and Krbetschek (2003b). They recognized that K-feldspar samples, bleached with a solar simulator, show a very strong phosphorescence at 865 nm. For a sediment sample with a palaeodose of ~1,500 Gy, extrapolation of the phosphorescence signal at room temperature using an exponential decay shows that its effect lasts beyond 1,000 s after bleaching (cf. Fig. 6 in Erfurt and Krbetschek, 2003b). To accommodate this effect in IR-RF measurement protocols, Erfurt and Krbetschek (2003b) recommended a pause of one hour after bleaching, before starting the next IR-RF measurement. In contrast, Buylaert et al. (2012) showed that after bleaching the phosphorescence signal intensity is lower by two orders of magnitude than IR-RF, its effect on the main IR-RF signal will be negligible. However, it should be noted that their setup differs from the one used by Erfurt and Krbetschek (2003b) (Sec. 3). Varma et al. (2013) reported that although the IR-RF signal of their sample was almost at its saturation level, it did not show significant phosphorescence after bleaching the sample for 800 s. Hence, they concluded that no extra pause is needed and suggested that a delay of 500 s is sufficient to reduce the phosphorescence down to the background level if the bleaching time is less than 800 s. Similarly, Schaarschmidt et al. (2019) reported a weak phosphorescence compared to the IR-RF signal and reduced the pause to 900 s for their samples. In summary, it seems that phosphorescence caused by bleaching can be avoided by introducing a pause of 15 min to 1 h prior to IR-RF measurements (Erfurt and Krbetschek, 2003b; Frouin et al., 2015; Schaarschmidt et al., 2019) in the case of solar simulator bleaching and may not be required if the sample is bleached with a UV LED for 800 s or longer (Varma et al., 2013).

Radiophosphorescence is a known phenomenon used in the past to characterize luminescence spectra from feldspar (e.g., Krbetschek and Rieser, 1995; Baril and Huntley, 2003b). Varma et al. (2013) observed phosphorescence with an intensity of ~35 % of the IR-RF signal (cf. Fig 2b in Varma et al., 2013) immediately after irradiation up to 800 Gy. Phosphorescence caused by irradiation can be a severe issue since IR-RF measurements need continuous irradiation during signal measurement. Thus, phosphorescence superposition onto the main IR-RF signal can be problematic and might be as high as 35 % of the IR-RF signal (Varma et al., 2013). Nevertheless,

if the phosphorescence intensity is independent of the previously administered radiation dose, it might be neglected. In contrast, if the radiophosphorescence is dose-dependent, it will be impossible to isolate it from the IR-RF signal. This possible superposition of IR-RF and radiophosphorescence needs to be further investigated.

Figure 7

(Phosphorescence)

5.4 IR-RF sensitivity

Schilles and Habermann (2000) conducted a bleaching study on natural and commercially available K-feldspar samples. Two repeated cycles of 20 h of sunlight bleaching resulted in different IR-RF intensities and changes in the shape of the decay curve for each bleaching cycle. Natural and commercial samples showed different bleaching levels and a relative change of signal intensity of 3.6–4.8 % for natural sunlight and 5.1–8.9 % for artificial solar simulation (SOL2, Hönle). These variations in signal intensity indicated sensitivity changes due to bleaching and/or irradiation during the measurement. In order to cope with this, Schilles (2002) suggested using a separate aliquot and measuring its IR-RF for two bleaching cycles. Based on these additional measurements, a dimensionless correction factor could be derived from the ratio of the regenerated IR-RF intensities (Fig. 8A).

Similarly, Varma et al. (2013) reported sensitivity changes during measurement and could not recover a given dose using IR-RF. They derived a sensitivity correction factor F_S by repeating the bleaching and regenerative IR-RF six times. F_S (also Sec. 6.1) is estimated from the ratio of IR-RF intensity of the first regenerated cycle to the extrapolated intensity of the zeroth cycle (Fig. 8B). Furthermore, Varma et al. (2013) recognized that all six sediment samples investigated in their study needed a sensitivity correction to obtain reasonable dose recovery results. Erfurt and Krbetschek (2003b) also showed a shape mismatch and change in intensity for multiple measurements but demonstrated that this sensitivity change would only affect the dose estimation by 3 % (cf. Fig 4 in Erfurt and Krbetschek, 2003b). In addition to these studies, Buylaert et al. (2012) mentioned the possibility of a significant sensitivity change, either induced by bleaching or by the IR-RF measurement itself.

Frouin et al. (2017) reported on a curve shape mismatch between the natural IR-RF (RF_{nat}) and the regenerated IR-RF (RF_{reg}) curve (cf. Fig. 2 in Frouin et al., 2017), and rejected the measured aliquots (Fig. 8C). In the literature, two attempts have been made to explain this behaviour: Kreutzer et al. (2017) gave evidence that a technical artefact with the measurement equipment caused an unwanted geometry change. Murari et al. (2018) investigated the possible reason for this shape mismatch using three modern bleached samples in a dose recovery study. For these samples, a given dose was recovered using the RF_{nat} and RF_{reg} signals. In their study, RF_{nat} refers to IR-RF curves from the naturally bleached modern sample, and RF_{reg} refers to IR-RF curves measured after bleaching with the solar simulator. As samples are bleached in both cases, both IR-RF curves, RF_{nat} and RF_{reg} , can act as regenerated IR-RF curves. An offset of 23 % was observed when the dose was recovered from the RF_{nat} signal (cf. Fig. 2 in Murari et al., 2018) while all the samples were able to recover the known dose from the RF_{reg} signal with an uncertainty of 4 %. Their findings showed the discrepancy in dose recovery and the mismatch of the shape of RF_{reg} curves compared to RF_{nat} curves. The latter is attributed to the change in IR-RF sensitivity. Possible causes for these sensitivity changes are the high photon flux of the built-in solar simulator, the high laboratory dose rate and/or the interference from other neighbouring peaks with the main IR-RF signal (i.e., 710 nm and 910 nm emissions; Trautmann, 1999; Erfurt and Krbetschek, 2003b). In summary, it seems that IR-RF is affected by sensitivity changes that should be monitored and corrected. Based on their findings, Murari et al. (2018) suggested a new analysis and correction method named the ‘*horizontal and vertical correction*’ method (Sec. 6.2).

Figure 8

(Sensitivity change monitoring)

5.5 IR-RF initial rise

A few IR-RF studies mentioned an unexpected signal rise at the beginning of the IR-RF measurement (e.g., Schilles, 2002; Buylaert et al., 2012; Frouin, 2014; Huot et al., 2015; Frouin et al., 2017). It was often described as a bump, a TL-like peak or an initial rise of the RF signal (Fig. 9A; for further discussions on the dynamic range see below) and it typically persisted for the first few hundred seconds (~6–12 Gy) before the IR-RF starts decaying monotonically (Huot et al., 2015). According to Frouin et al. (2017), the initial rise in the natural signal seemed to be positively

correlated with the equivalent dose (D_e) (cf. Fig. S7 in Frouin et al., 2017) of a sample and was observed for every K-feldspar sample used in their study.

In contrast, the Freiberg group never reported such IR-RF behaviour (e.g., Krbetschek et al., 2000; Erfurt, 2003b) leading to speculation that differences in instrumental design (overall system efficiency, different detection bandpass filter combinations or radiation source strengths) may cause the effect or favour its detection. Measurements using both commercial devices (*lexsyg research* and *Risø*, Sec. **Error! Reference source not found.**) showed the initial rise behaviour (e.g., Huot et al., 2015; Frouin et al., 2017; Qin et al. 2018). However, this is not discussed in detail by Buylaert et al. (2012) who discarded the signal corresponding to the first ~20 Gy from their data analysis considering it as a sample-specific behaviour.

Huot et al. (2015) thoroughly investigated the origin of the initial rise after bleaching (regenerated signal). They hypothesized that the rapid increase in RF observed at the beginning of the irradiation, is not due to higher electron trapping, but can be explained by thermally assisted phosphorescence. “Minute variations in sample temperature” (Huot et al., 2015, p. 241) can cause this peak because of the existence of shallow traps which emit phosphorescence in the near-infrared region. Their recommendation to avoid this peak was to wait at least 1 h after bleaching, let the sample cool down to room temperature, or measure IR-RF at elevated temperatures of around 70 °C to 100 °C. Nevertheless, the phenomenon does not seem to disappear from the IR-RF signal even when measured at elevated temperatures of 70 °C and waiting for one h after bleaching (cf. Fig. 2 vs Fig. 7 in Frouin et al., 2017).

Furthermore, the reported a correlation between the intensity of the initial rise in the natural signal and the sample's D_e (cf. Frouin et al., 2017 their Fig. S7), indicated that shallow TL traps alone cannot explain this phenomenon. Nevertheless, from the perspective of dating, it seems that the effect of the initial rise does not affect dose estimation as it appears only for 100 s to 200 s (typically ~6–12 Gy) in every IR-RF signal (i.e., natural and regenerated IR-RF signals). However, further investigations combined with modelling are needed to better understand the origin of the IR-RF signal increase during the first seconds.

Figure 9

(Initial rise and dynamic range)

5.6 IR-RF signal stability

The IR-RF signal stability has two dimensions: thermal stability and athermal stability. The first is directly related to the depth of the trap and represents the stability of the electrons captured by the defect over time, dependent on the ‘burial’ temperature. The second, also known as ‘anomalous fading’ (Wintle 1973), is temperature independent.

The thermal stability of the IR-RF signal was investigated by Trautmann et al. (1999a) who used pulse annealing experiments, and they reported thermal stability of the IR-RF signal up to 450 °C (Fig. 10A). However, this result was observed only for one sample (Ook1), which is >1 Ma old; two younger samples showed a decrease in signal intensity after 250 °C (Fig. 10A). Later experiments by Erfurt and Krbetschek (2003b) and Frouin et al. (2017) (Fig. 10B) confirmed these findings. Further, it was noticed that for temperatures of 250 °C and higher, natural IR-RF (RF_{nat}) signal intensities decreased with pulse annealing temperature (Fig. 10B) while they increased slightly for regenerated IR-RF signals (RF_{reg}). If annealing at high temperatures resets the IR-RF signal, the IR-RF intensity should not decrease, which is in accordance with observations on RF_{reg} , but in contradiction to that for RF_{nat} . This contrasting feature may be explained by a change of the IR-RF sensitivity with temperature. In thermoluminescence (TL) studies on K-feldspar rapid, temperature-induced luminescence sensitivity decreases were frequently reported (Aitken, 1985a, 1998). Those changes are non-repeatable in subsequent dose cycles (cf. reasoning in Frouin et al., 2017).

Nevertheless, while temperatures above ca. 250 °C may impact the D_e , these observations should not be used to draw general conclusions on the thermal stability of the defect responsible for the IR-RF emission. Erfurt (2003a, b) referred to works on amazonite (cf. Ostrooumov, 2016 for an overview) and argued that the Pb^{+} centres are stable up to ~450 °C (Speit and Lehmann 1982) or even up to 700 °C (assumption in Erfurt, 2003b: 500 °C; 700 °C in Ostrooumov, 2016). Above this temperature, the Pb^{+} centre disappears (a process also referred to as de-amazonitization).

Krbetschek et al. (2000) presented experimental results supporting the hypothesis of long-term stability of the IR-RF signal. For instance, short-term (days to months) fading tests with storage of samples for several months at room temperature showed no sign of signal increase (i.e., no emptying of traps) which seems to confirm signal stability over short periods (at room

temperature). Furthermore, based on the dating of sediment samples using IR-RF, e.g., Wagner et al. (2010) and Novothny et al. (2010) claimed that the IR-RF signal exhibited no indication of fading for ages in the range ca 420–700 ka (Wagner et al., 2010) and 148–250 ka (Novothny et al., 2010). Likewise, Frouin et al. (2017) and Kreutzer et al. (2018a) reported a good agreement with the independent age control of even older ages. By contrast, Buylaert et al. (2012) showed age underestimation for older samples (>100 ka) and overestimation for younger samples (< 50 ka). They speculated whether the offset could be explained by signal instability (fading), bleachability and sensitivity change during measurement. They also showed the natural IR-RF signal from an infinitely old sample was only 84 % of the saturation, suggesting the signal might fade. However, the measurement setup by Buylaert et al. (2012) did not match the suggestions by Erfurt and Krbetschek (2003b), e.g., regarding the detection window, and should be read cautiously. Recently, Kumar et al. (2021) reinterpreted the findings by Buylaert et al. (2012). They reported IR-PL age results in agreement with independent age control. These findings indicate that IR-PL does not suffer from athermal fading or signal instability. However, since Kumar et al. (2018) hypothesised a similar trap for the IR-PL and the IR-RF, they concluded that IR-RF does not suffer from signal instability. Hence, without presenting new IR-RF data, Kumar et al. (2021, p. 14) concluded: “[...] *that the under-estimation in IR-RF [meant are the results reported by Buylaert et al., 2012] is likely because of sensitivity changes rather than signal stability.*” Nevertheless, beyond the research summarized above, further studies should be carried out to investigate the thermal and athermal stability in the context of IR-RF as a luminescence dating method. For IR-PL, Kumar et al. (2021) suggested tests on geological samples (~ Ma), i.e. samples in apparent dose saturation, which might also provide a good test for the IR-RF signal stability in future studies.

Figure 10 A B

(Signal stability)

5.7 IR-RF dose limits

The minimum measurable dose has not yet been systematically determined with IR-RF. While Erfurt (2003b) estimated a dose of ca 40 Gy, Frouin et al. (2017) reported measurable doses of 0.5 ± 1.0 Gy and 1.2 ± 1.9 Gy for two modern analogue samples. Current instrument configurations

allow signals with a few photon-counts per second to be distinguished. In available luminescence measurement systems (Sec. 3), the IR-RF signal of K-feldspar is usually of the order of a million photon counts per second with signal intensities at its maximum when the sample is bleached, i.e., for zero dose samples. Thus, the minimum measurable dose (limit) is a function of stimulation dose-rate (Gy s^{-1}), the measurement channel resolution (s channel^{-1}) and the applied statistical procedure to distinguish two bright signals and determine the D_e (e.g., the sliding method causes discretization effects, Sec. 6.2). For example, a sampling rate as applied by Murari et al. (2018) of $10 \text{ s channel}^{-1}$ for a dose rate of ca. 0.06 Gy s^{-1} would theoretically correspond to a minimum distinguishable dose of 0.6 Gy on average.

The IR-RF dynamic range is defined as the ratio of the maximum to the minimum of the IR-RF signal intensity. In other words, this is the ratio of the IR-RF signal from saturation to the bleaching level of the sample, which in general varies about a factor of 2 (Erfurt and Krbetschek, 2003a). The IR-RF signal dynamic range is minimal (Fig. 9B) compared to the signal dynamics from the other variants of luminescence such as OSL or IRSL, where it typically is at least an order of magnitude higher. Due to low signal dynamic ranges, the slope of IR-RF intensity (I) with respect to dose (D_e) changes gradually and finally approaches zero. In terms of resolving dose estimates, the resolution becomes impoverished in the higher dose region as a slight change in intensity (dI) may lead to a large uncertainty in dose estimation (dD_e). Erfurt and Krbetschek (2003b) recommended determining the dose where the slope of signal intensity vs dose approaches a value of zero (i.e., $dI/dD_e \approx 0$). Based on this parameter, they found that for their reader configuration, IR-RF curves allow dose estimation up to $\sim 650 \text{ Gy}$.

However, the upper dose limit of IR-RF, and with it, the temporal range, is subject to ongoing research. Krbetschek et al. (2000) reported a saturation D_e value of $1,440 \pm 215 \text{ Gy}$ (nature of the error not reported) for a single sample, and in a recent IR-RF dating study Kreutzer et al. (2018a) reported a measurable mean dose of $1,064 \pm 41 \text{ Gy}$ (mean \pm standard deviation). Erfurt (2003b) estimated a mean saturation dose as high as $1,500 \text{ Gy}$. However, Erfurt (2003b) and Erfurt and Krbetschek (2003b) also estimated the maximum resolvable dose at 600 Gy to 650 Gy as the small IR-RF signal dynamic range can limit the precision of signal interpolation. The highest, single aliquot, IR-RF dose of $4,181 \pm 371 \text{ Gy}$ (mean \pm standard deviation) was reported by Wagner et al.

(2010) (cf. their “Supporting Information”, Table S2) using the same instrument as Erfurt et al. (2003).

On a *lexsyg research* system Frouin et al. (2017) recently reported successful measurement of a ~2,100 Gy dose using a regenerated IR-RF signal that was recorded up to 4,000 Gy cumulative dose (cf. their Fig. 7 for sample TML1). Furthermore, Murari et al. (2018) demonstrated accurate laboratory dose recovery up to 3,600 Gy by interpolating onto a regenerated IR-RF curve measured up to 3,900 Gy. However, it should be pointed out that the intensity difference between 2,000 Gy and 3,500 Gy was only around 4 % (Fig. 9B for the dynamic range of IR-RF), which leaves the results susceptible to minimal intensity changes. Hence, at this moment, we cannot refer to a saturation limit of IR-RF. However, the one single value published by Murari et al. (2018) of ca. 3,600 Gy would allow age determinations (dose rates in the order of 2–3 Gy ka⁻¹) of 1.2 Ma to 1.8 Ma. Whether this dose (and temporal) range is feasible for routine dating is still under debate.

5.8 The IR-RF alpha-efficiency

The ionisation efficiency and, with it, the efficiency of induced luminescence per unit dose, depends on the type of irradiation (i.e., α - vs β - vs γ -radiation). Commonly, the luminescence produced by α -particles per unit dose is substantially lower than for β - or γ -radiation. Thus, the α -efficiency needs to be determined to correctly calculate the β -equivalent α -dose rate contribution (cf. Aitken, 1985a) if polymineral fine grain (4–11 μ m) or other grain size fractions untreated with HF are used. So far, only a single study exists determining the α -efficiency of K-feldspar using IR-RF. Kreutzer et al. (2018b) used an α -flux calibrated ²⁴¹Am source. The central S_α -value (Guérin and Valladas, 1980; Valladas and Valladas, 1982) obtained from four fine-grain K-feldspar samples (84 aliquots) was $9.26 \pm 1.62 \mu\text{Gy}/(10^3 \alpha \text{ cm}^{-2})$. The corresponding (dimensionless) value in the a -value system (cf. Aitken 1985b) of 0.067 ± 0.012 is similar to a -values reported for IRSL polymineral fine grain (e.g., Kadereit et al., 2010). Based on these findings and if the α -efficiency cannot be determined, an estimated a -value of 0.07 ± 0.01 (applied to fine grain and unetched coarse grains, cf. Kreutzer et al., 2018b) appears to be justified.

6 Measurement protocols and data analysis

Like other luminescence measurement protocols for equivalent dose (D_e) determination (e.g., for TL, OSL or IRSL), over the years, several measurement protocols and data analysis techniques have been proposed to determine the D_e for IR-RF.

6.1 IR-RF measurement protocols

The first comprehensive IR-RF measurement protocol named IRSAR (infrared single-aliquot regenerative-dose) was presented by Erfurt and Krbetschek (2003b). Frouin et al. (2017) introduced a modified version of this protocol and entitled it RF₇₀ (where the subscript '70' refers to the applied measurement temperature of 70 °C). Additionally, several other protocols have been reported in the literature and are summarized in Table 6.

Table 6

(Measurement protocols)

All listed protocols consist of less than six measurement steps. Common to all protocols are three main steps: (I) measurement of the natural IR-RF signal (RF_{nat}), (II) signal resetting by bleaching and (III) measurement of the regenerated IR-RF (RF_{reg}) signal after bleaching. The duration of the IR-RF measurements (natural, regenerative) is determined by the chosen data analysis approach (Fig. 11). For example, D_e determination via curve fitting and signal extrapolation results in IR-RF measurements of longer duration for the natural IR-RF signal than for the regenerated signal and vice versa for a D_e determination via interpolation.

Trautmann et al. (1999a), Krbetschek et al. (2000) and Schilles (2002) distinguished between an additive (extrapolation) and a regenerative (interpolation) measurement approach, depending on the particular IR-RF signal (natural: additive; regenerative: regenerative) used for subsequent curve fitting. However, this distinction is misleading and should be avoided as it conflicts with the commonly accepted terminology used for TL/OSL. All recorded IR-RF signal curves are dose-response curves, and signal resetting is carried out by optical bleaching. Thus, natural IR-RF curves are always additive dose-response curves, irrespective of the technique used to analyse the data and to obtain the D_e , namely: extrapolation, interpolation or sliding (see the following section).

Bleaching duration: All published protocols include an optical bleaching step to reset the natural IR-RF signal. The bleaching is either carried out by using an artificial light source or by natural sunlight. To mimic natural sunlight conditions, Frouin et al. (2015) proposed a bleaching spectrum consisting of six different wavelengths ranging from UV-A (365 nm) to NIR (850 nm), while Buylaert et al. (2012) used only a single wavelength (UV-violet LED, 395 nm) to reset the IR-RF signal. The bleaching duration is sample dependent and linked to the technical specification of the equipment, the available wavelengths, and power. Using a similar measurement setup, Varma et al. (2013) and Buylaert et al. (2012) found bleaching for 800 s and 1,500 s respectively, to be sufficient for most cases, Frouin et al. (2017) suggested solar simulator bleaching for at least 10,800 s. Kreutzer et al. (2018a) suggested a bleaching test using the internal solar simulator of their *lexsyg* system. The test applied consecutive bleaching steps of 1,000 s each. A stable signal plateau indicates sufficient bleaching. Generally, it appears that longer bleaching times should be preferred to ensure the resetting of the natural IR-RF signal. For further details on the bleaching behaviour of the IR-RF signal see Sec. 5.2.

Pause duration: Five out of seven IR-RF protocols (Table 6) suggested a pause after the optical resetting of the IR-RF signal for at least 1,800 s. The pause is believed to account for an unwanted superposition of IR phosphorescence on the IR-RF signal (e.g., Erfurt and Krbetschek, 2003b). Varma et al. (2013) carried out the pause as a phosphorescence measurement just before the stimulation itself. Based on their results, it appears that the phosphorescence is induced only by the irradiation ('radiophosphorescence') and that it is not further increased by bleaching. They thus proposed an optimum bleaching time of 800 s to reduce phosphorescence to its residual level without implementing an additional pause within the measurement procedure. However, this study contradicted the observation made on the same system (*Risø* TL/OSL DA-20 with IR-RF attachment) by Buylaert et al. (2012) who showed the appearance of IR phosphorescence even after bleaching of 1,500 s, though it was two orders of magnitude smaller than the IR-RF signal which can probably be considered negligible. Nevertheless, other studies contradicted these findings, e.g., Erfurt (2003b), Erfurt and Krbetschek (2003b) and Huot et al. (2015) showed the presence of phosphorescence directly emitted after bleaching. The above-described observations suggest that an additional pause of 30 min up to 1 h might be beneficial to minimize the potential

effects of unwanted signal superposition from the phosphorescence caused by bleaching (also Sec. 5.3).

Preheat and measurement temperature: The work of Trautmann (1999) gave evidence for a strong temperature dependence of the IR-RF signal of K-feldspar, which appears to be related to the sample's age (see also Erfurt, 2003b). Considering the dependency of the IR-RF signal intensity (Trautmann, 1999; Erfurt, 2003b; Frouin, 2014) on the preheat and measurement temperature, measurements under well-controlled temperature conditions appear advisable. However, due to technical limitations, measurements under controlled (elevated) temperature conditions have only been applied by Frouin et al. (2017). They suggested a preheat of 70 °C based on the observation of thermally assisted phosphorescence. Huot et al. (2015) advised that a temperature range of 70 °C to 100 °C would be suitable. However, Erfurt and Krbetschek (2003b) neglected the need for any preheat prior to measurement following their observation of no change in IR-RF intensity from room temperature to 250 °C (cf. Fig. 2 in Erfurt and Krbetschek, 2003b). Nevertheless, a comparison of IR-RF ages with independent age control showed improvement in results when measurements are carried out at elevated temperature (Frouin et al., 2017). Therefore, Frouin et al. (2017) recommended measurements at elevated temperature.

Sensitivity correction (also Sec. 5.4): Monitoring changes in the dose-response characteristics is an essential feature of every OSL SAR protocol. Schilles (2002) and Varma et al. (2013) included treatments to correct for unwanted changes in IR-RF signal sensitivity by introducing a correction factor for IR-RF measurements. Murari et al. (2018) investigated a new way of correction. In this method, the shapes of IR-RF curves are matched by moving the RF_{nat} vertically along with horizontal sliding (Sec. 5.4 for sensitivity change). This method was able to recover a given dose with 3–10 % accuracy, compared to an offset by 15–23 % when recovered only using the horizontal sliding method proposed by Buylaert et al. (2012). The recommended method (Kreutzer et al., 2017; Murari et al., 2018) does not need any extra measurements other than those implemented in the protocol suggested by Frouin et al. (2017). However, the RF_{nat} measurement should be long enough to produce an RF signal with pronounced curvature to match the RF_{nat} and RF_{reg} curves.

6.2 Data analysis

Data analysis for D_e estimation is essential for age determination. D_e determination requires a comparison of the natural and a minimum of one regenerated IR-RF signal. The different methods available for making this comparison are described below.

Figure 11

(D_e determination methods)

Extrapolation and Interpolation method: Three different approaches were presented to analyse IR-RF data (Fig. 11): (I) extrapolation, (II) interpolation and (III) sliding. The first two approaches comprise a mathematical curve fitting for D_e determination. Extrapolation (Fig. 11A) and interpolation (Fig. 11B) requires that either the natural or regenerative signal is recorded over a more extended period (natural signal: extrapolation; regenerative signal: interpolation). The chosen channel resolution and stimulation time determine the precision of the curve fitting and thus, the statistical error of the D_e . For curve fitting (extrapolation, interpolation), Trautmann et al. (1999a), Krbetschek et al. (2000) and Schilles (2002) proposed a single exponential decaying function with three parameters. Later, Erfurt and Krbetschek (2003b) recognized that the curve shape could be best described using a so-called stretched exponential function (Fig. 12). This function was suggested in a general form by, e.g., Pavesi and Ceschini (1993). The stretched exponential function introduces a dispersion factor (β), which accounts for the underlying physical processes in disordered condensed matter systems. Unfortunately, the mathematical expression of this function type is not consistent in the IR-RF literature (Fig. 12) and differs regarding the placement of β in the equation. Although the functions shown in Fig. 12 may result in consistent D_e estimations, they reveal different curve shapes for similar parameter sets. Therefore, parameters describing an IR-RF curve's decay cannot be compared without a statement on the applied mathematical expression.

Figure 12

(Equations used for IR-RF curve fitting)

Due to the general difficulties associated with D_e estimation by extrapolation (i.e., substantial uncertainties), this methodological approach appears to have been abandoned in later studies, and

more recently only D_e estimation by interpolation has been applied (e.g., Wagner et al., 2010; Novothny et al., 2010; Kreutzer et al., 2014). Nevertheless, every fitting method requires an assumption regarding the IR-RF curve shape, either based on a model or the best graphic adaption of the curve shape. Furthermore, IR-RF curves recorded only for a short time do not sufficiently reveal the curve shape and potential changes.

Sliding method: Buylaert et al. (2012) suggested a data analysis method based on horizontal sliding of the RF_{nat} curve until the best match is reached (inspired by the *Australian slide* method introduced initially by Prescott et al., 1993). This approach appears to be even more justified since Frouin et al. (2017) pointed out an initial rise at the beginning of the natural IR-RF curve (Sec. 5.5). The observed initial rise at the beginning of the IR-RF curve does not allow an unbiased channel selection if curve fitting combined with interpolation or extrapolation is applied. In other words, for IR-RF data analysis, the (horizontal) sliding technique should be favoured over the curve fitting approach. However, it was often seen that RF_{nat} and RF_{reg} curves did not match after horizontal sliding. Kreutzer et al. (2017) suggested enhancing the technique by combining vertical and horizontal sliding to account for an observed IR-RF light level change encountered for a particular technical setup, presented in Murari et al. (2018). The sliding method requires a long natural IR-RF measurement to match the regenerative IR-RF, e.g., Frouin et al. (2017) (their supplement) recommended a minimum of 40 channels for robust D_e estimation for the horizontal sliding method. In the case of the vertical and horizontal sliding methods, Murari et al. (2018) used 100 channels. However, the precise number depends on the signal shape.

Error estimation: Krbetschek et al. (2000) suggested that the primary source of random error in the IR-RF ‘mean’ D_e arises from changes in the sample geometry at a single-grain level (see also Trautmann et al., 2000b). In contrast to OSL, where the dose-response curve is typically reconstructed with a few (e.g., 5–15) regenerative dose measurements, the number of channels used for constructing the IR-RF dose-response curve can be increased dramatically (e.g., >1,000 values) and is limited only by the instrumental signal-to-noise ratio and the total number of allowed channels by the system. Consequently, for IR-RF dating studies, individual (statistical) errors have been ignored, and the standard error deduced from individual D_e distributions (e.g., Wagner et al., 2010; Lauer et al., 2011; Kreutzer et al., 2014). To account for potential errors Frouin et al. (2017) (their supplement) developed an approach to estimate the standard error of an individual aliquot

based on a non-parametric bootstrapping approach (Efron, 1979) for the sliding method. Nevertheless, the results of Frouin et al. (2017) also showed that the obtained individual statistical standard error remains negligible in comparison to inter-aliquot scatter and becomes relevant only for dim IR-RF signals.

Data analysis software: To analyse IR-RF data, no specialized software is needed, and commercial software solutions, e.g., *SigmaPlot*TM or *ORIGIN*TM may be sufficient to analyse single measurements. However, within a dating study, the amount of data may demand more comprehensive and efficient solutions. Two freely available software solutions have been published to analyse IR-RF data based on the IRSAR Erfurt and Krbetschek (2003b) approach. The *MS Windows*TM software *RLanalyse* (Lapp et al., 2012; latest version 1.20) has implemented the (horizontal) sliding method and works with BIN/BINX-files produced by a *Risø* TL/OSL reader. The most recent version of the function `analyse_IRSAR.RF()` implemented in the package ‘Luminescence’ (Kreutzer et al., 2012, 2018c) makes use of the platform-independent programming language **R** (R Core Team, 2018), and supports the horizontal and vertical sliding approach. The function also supports D_e estimation via curve fitting as described by Erfurt and Krbetschek (2003b) as well as via sliding including the individual standard error estimation approach described in Frouin et al. (2017) and Murari et al. (2018). Through the ‘Luminescence’ environment, XSYG-files (Freiberg Instruments *lexsyg* readers), BIN/BINX-files (*Risø* TL/OSL reader) as well as various other data formats (e.g., file endings *.csv, *.txt) are supported as input data.

7 Application of IR-RF dating

The broader use of IR-RF as a dating method for sediments started mainly after introducing the IRSAR protocol by Erfurt and Krbetschek (2003b). Signal saturation levels of $> 1,000$ Gy (e.g., Erfurt and Krbetschek, 2003b and Sec. 5.7) favoured IR-RF dating applications on Middle Pleistocene sediments which are generally beyond the quartz OSL dating limit. The typical dose saturation for quartz OSL measured in the UV is reached around 150–200 Gy (Wintle and Murray, 2006) except for a few cases where quartz doses > 300 Gy are reported (e.g., Lowick and Valla, 2018). Until now, IR-RF dating has mainly been applied to coarse grain K-rich feldspar using multiple-grains (Secs. 7.17.2). Spatially resolved and single grain studies are limited to preliminary

work (e.g., Schilles 2002; Trautmann et al., 2000b) and a manuscript in an open discussion by Mittelstrass and Kreutzer (preprint) and are thus not further discussed here. Applications of IR-RF on polymineral fine-grain samples (4–11 μm) are currently limited to three studies (Schilles, 2002; Kreutzer et al., 2018b; Coussot et al., 2019).

7.1 Application to glacio-fluvial and fluvial sediments

In the past, IR-RF dating has been favoured particularly for constraining the timing of the Saalian glacial cycle and the Eemian interglacial by dating fluvial deposits of sites located in Central/Eastern Germany (Eissmann, 2002) by Degering and Krbetschek (2007), Krbetschek et al. (2008) and Kreutzer et al. (2014). Degering and Krbetschek (2007) presented IR-RF ages ranging from 120 ± 15 ka to 158 ± 21 ka for the Eemian site Klinge (Germany), and the results were in good agreement with quartz and K-feldspar OSL and IRSL luminescence dating results. IR-RF dated fluvial sites (e.g., Wallendorf and Delitzsch, Germany) are highly relevant for establishing a chronology for Middle Pleistocene Palaeolithic human activity in Europe due to the presence of stone-artefacts embedded in fluvial sands and gravels. Krbetschek et al. (2008) presented IR-RF ages ranging from ~ 150 ka to ~ 306 ka for the Saalian period and highlighted human activity in Central Germany already at around 300 ka. Lauer and Weiss (2018) compared pIRIR₂₉₀ luminescence ages from the important palaeolithic site of Markkleeberg (Baumann et al., 1983; Schäfer et al., 2003) with previously available IR-RF ages (Krbetschek et al., 2003) and found the pIRIR₂₉₀ and IR-RF ages were in excellent agreement and provided late MIS 6 ages for the upper fluvial sequence at the site. Also, for the key site of the Homo heidelbergensis, located at Mauer in south-west Germany, IR-RF was applied to fluvial deposits correlated to the archaeological horizon of the Mauer mandible. At this site, the IR-RF ages were in good agreement with results of combined electron spin resonance (ESR)/U-series dating on mammal teeth, yielding an age of around 0.6 Ma (Wagner et al., 2010). Lauer et al. (2011) used IR-RF to date fluvial deposits collected from sediment-cores drilled into the northern Upper Rhine Graben (Germany). They deduced several fluvial aggradation periods and phases of increased tectonic subsidence between ~ 300 ka and ~ 650 ka based on these IR-RF ages. Li et al. (2017) compared the data reported by Lauer et al. (2011) with their chronology based on fading corrected pIRIR₂₂₅ ages obtained for the core Heidelberg UniNord 1. Except for the lowermost sample (below the B/M boundary) both chronologies were broadly consistent. For the lowest sample, Li et al. (2017) reported a minimum

age of $>602 \pm 77$ ka, consistent with the magnetostratigraphic information which was not available in 2011. In light of the new findings, the IR-RF age of 643 ± 28 ka by Lauer et al. (2011) should be considered as minimum age. The reasons for this age underestimation should be subject to future research.

In general, studies presented by Krbetschek et al. (2008) and Wagner et al. (2010) demonstrated good agreement with independent age control. In contrast to these studies, Buylaert et al. (2012) showed that IR-RF dating results of coastal marine sediments from Russia and Denmark as well as colluvial sediments from France were either overestimated (for ages between 20–45 ka) or underestimated (for older samples ~ 128 ka) compared to independent dating methods based on biostratigraphy, radiocarbon (^{14}C), OSL and pIRIR₂₉₀ (for numerical values cf. Table S1 in Buylaert et al., 2012).

Figure 13 ABC
(Age comparison)

7.2 Application to aeolian deposits

Well-bleached sediments, such as wind-blown loess or dune sands seem to be most suitable for IR-RF dating applications, although the amount of sand-sized K-feldspars in silt-dominated loess is limited. Early aeolian samples used for IR-RF dating result originate from a sediment core from the Gaxun Nur Basin in North-West China (Wünnemann et al., 2007). The IR-RF dating results² significantly overestimated previously reported TL/IRSL ages and were discarded by the authors (Wünnemann et al., 2007), without presenting further technical details.

Novothny et al. (2010) were the first to extract coarse-grained K-feldspars from Hungarian loess for IR-RF dating. The IR-RF ages of ~ 200 ka presented by Novothny et al. (2010) significantly overestimated the fading-corrected IRSL ages of ~ 130 ka, explained due to insufficient bleaching of the coarse-grained fraction. An IR-RF age overestimation compared to quartz OSL ages of reworked aeolian sediments from Egypt was also reported by Buylaert et al. (2012), which was either attributed to a preliminary determination of the bleaching level before the regenerative dose

² In Fig. 22.3 (Wünnemann et al., 2007) the IR-RF results were erroneously presented as OSL dates.

measurement or sensitivity changes between the measurement of the natural and regenerated curves.

It was recently demonstrated that the modified IRSAR-protocol, measuring the IR-RF signal at 70 °C (RF₇₀), recovered IR-RF ages on modern aeolian samples that agreed with independent age control. Frouin et al. (2017) have shown reasonable agreement with independent age control from polymineral (4–11 µm) fine-grain results published by Meszner et al. (2013). However, they also observed a large scatter in their D_e distributions. Another age from a loess sample from the same site appeared to be underestimated. This offset was explained by the low D_e values resulting from low signal intensities (Frouin et al., 2017).

Kreutzer et al. (2018a) presented a dating application study on coastal dynamics from the Médoc region (south-west France), comparing coarse grain K-feldspar IR-RF ages (RF₇₀ protocol) with quartz OSL ages and quartz multiple-centre ESR dating (Toyoda et al., 2000). In this study, the IR-RF ages were systematically older than the SAR quartz ages, which was believed to be a consequence of insufficient resetting of the IR-RF signal. However, this study showed reasonable agreement with the ESR ages for older sediments (200–330 ka). Similarly, Scerri et al. (2018) also found that RF₇₀ and pIRIR₂₉₀ age estimates were consistent within a 2-sigma limit and in stratigraphic order. The aeolian samples from an archaeological site in Saudi Arabia resulted in age estimates of ~276 ka for the older (archaeologically sterile) layer and 197 ka for the human occupation layer.

7.3 Remarks on IR-RF age accuracy and independent age control

Figure 13 presents a non-exhaustive overview of published IR-RF data. The ages from the IR-RF dating approaches generally show good agreement with independent age control (e.g., Degering and Krbetschek, 2007), whereas the IR-RF ages from Buylaert et al. (2012) disagree with independently derived ages. Again, a good agreement between IR-RF and independent ages was reported using a modified IRSAR protocol (RF₇₀) suggested by Frouin et al. (2017).

The study by Frouin et al. (2017) was the first to present various IR-RF dating applications with a modified IRSAR protocol (RF₇₀), which agreed with independent age control. IR-RF dating of a Pleistocene beach deposit from Peru and colluvial deposits from France appeared to be overestimated compared to independent age information from IRSL, U/Th series or radiocarbon

dating; a pattern also observed by Schaarschmidt et al. (2019). However, for the Peruvian sample, IR-RF and pIRIR₂₉₀ ages agreed within error limits. Similarly, Holocene beach sand from Denmark and another colluvial example from France yielded ages in good agreement with independent age information. In conclusion, published IR-RF dating results indicated that the IR-RF dating method produced correct ages in some cases, but fails for other cases. It seems that there are still methodological problems related to IR-RF dating, and further investigation is needed to overcome these challenges.

8 Summary and future directions of IR-RF dating

Overall, regardless of ambivalent dating results in some studies, IR-RF appears to be a promising but somewhat overlooked dating method on K-feldspars. The status quo renders a picture with several, potentially, game-changing advantages but without a significant breakthrough because those benefits are not received as significant enough by dating practitioners. On the other hand, IR-RF poses a bunch of open questions and challenges that are yet to overcome.

8.1 The status quo

The plus side of IR-RF dating has different dimensions. From a **methodological perspective**, IR-RF is believed to monitor the trapping of electrons in the principal trap, i.e., it is a *direct* measurement of the dose accumulation in the mineral. This approach is conceptionally different from conventional OSL, IRSL and TL measurements, involving secondary recombination processes to infer the signal of interest. Debated methodological issues, such as phosphorescence and sensitivity change (see Secs. 5.35.4), appear to be manageable by proper experimental and data analysis design.

From a **practical perspective**, compared to post-IR IRSL dating, for instance, the measurement sequence for one aliquot is reasonably concise, less error-prone, and, depending on the aimed dose range, likely less time-consuming (depending on the chosen measurement sequence). The dose-response curve is the IR-RF curve measured during irradiation with a resolution usually in the order of a fraction of a Gy. Instead of applying different fitting equations determining the D_e , the data analysis using the sliding method, i.e., matching two dose-response curves (RF_{nat} and RF_{reg}), could not be more straightforward. Software to analyse IR-RF signals is freely available and partly

open-source. The biggest obstacle for applying IR-RF dating in the past, availability of equipment, is no more. At least two commercial manufacturers offer ready-to-use IR-RF readers for research and dating applications.

From a **dating perspective**, the target mineral, K-feldspar, shows a high natural abundance, an acknowledged higher luminescence dating range compared to quartz, and the internal potassium concentration lowers the impact of the external dose-rate contribution. However, conventional feldspar luminescence is reported to suffer from an unwanted athermal signal loss (fading). Contrary to IRSL, no definite evidence was provided for fading of the IR-RF signal of K-feldspars to date. Although Buylaert et al. (2012) reported age underestimations for older samples of ca 30 %, this does not appear to be a generally observed pattern. Furthermore, signal instability as a cause for this observation was considered unlikely by Kumar et al. (2021). The thermal stability of the IR-RF signal (determining the potential age range) appears to be sufficiently high up to 700 °C (Sec. 5.6), though previous experiments indicated changes of the IR-RF signal shape above ~250 °C (Trautmann et al., 1999a; Erfurt and Krbetschek, 2003b; Frouin et al., 2017).

However, to sustain, a dating method has to show advantages over established methods, which are also perceived as significant for application studies. Supposing that the signal of choice is thermally and athermally stable, for luminescence-based chronologies such advantages are measured in terms of bleachability and temporal range.

Compared to pIRIR₂₉₀, which seems to suffer from no or at least less fading than IRSL, IR-RF's bleachability is comparable. In other words, in natural environments involving sediment transport processes with only short sunlight exposure, IR-RF dating seems to be as applicable as pIRIR₂₉₀ and other methods may suit better. Whether the temporal range is as high as the ~1.2–3 Ma (~3,600 Gy) postulated by Murari et al. (2018) is yet to be revealed. More realistically seem values around up to 1,500 Gy measured by, e.g., Erfurt (2003b), Frouin (2014), Frouin et al. (2017) and Kreutzer et al. (2018). Here we conclude that the signal saturation limit (and thus the temporal range) appears to be significantly higher than for conventional OSL on quartz (up to 400 Gy, typically lower, for a review cf. Wintle and Adamiec, 2017). This “winning margin” is less pronounced if IR-RF is compared to studies reporting post-IR IRSL (more specific: pIRIR₂₉₀) or MET-pIRIR results. For instance, Liu et al. (2016) reported doses up to ca. 1,240 Gy, however,

ages were reported to underestimate the independent age control above ca. 600–900 Gy (cf. Lieu et al., 2016; their Table 2 and Fig. 3). For MET-pIRIR, Li et al. (2014) reported potential natural dose measurements up to ca. 1,500 Gy, however, it remains unclear whether such values can be met regularly in routine dating studies (cf. Zhang and Li, 2020 for a discussion).

8.2 Future directions

Future methodological research on IR-RF should first resolve some open debates, particularly on signal saturation and signal stability (fading). Although fading does not appear to be a generally observed pattern, this topic should be explored in more detail, along with potential sensitivity changes using samples of known and geological age. The biggest obstacle to resolving whether the signal recorded with IR-RF is stable or suffers from an athermal signal loss over geological timescales might be the experimental design. From the current perspective, it appears that short experiments over a couple of weeks to months are not sufficient to provide answers to that question. Hence, research should involve laboratories with a relatively long history and an archive of already measured, irradiated and stored feldspar specimen. The quantification of the saturation level is more of theoretical than practical relevance.

With regard to the literature, it is safe to assume a rather broad, sample dependent, saturation level range between 600 Gy and 2,000 Gy up to perhaps 4,000 Gy. However, of relevance for the dating practice is the limit of the K-feldspar sample at hand, regardless of any theoretical value. In other words, the saturation level of IR-RF dating and with it the temporal range, will itself establish circumstantially over time; with or without dedicated research. However, both research on the fading behaviour and the signal saturation might contribute to a broader understanding of the physics underpinning IR-RF. To date, Trautmann's model (Trautman et al., 2000a) remained, to our knowledge, the only comprehensible model genuinely dedicated to IR-RF. Clearly, efforts are needed to combine the old and new findings around IR-PL and combine them with established knowledge in IRSL to decipher the proposed resemblance of IR-RF and IR-PL (cf. Kumar et al., 2020). Similarly, while there seems to be extensive research to identify the defect responsible for IR-PL (most recently Kumar et al., 2020), it appears that established knowledge on the role of Pb in the luminescence production in feldspar (cf. textbook by Ostrooumov, 2016) did not (yet) receive full attention.

On the application site, the next logical application step is spatially resolved IR-RF in a single grain (Mittelstrass and Kreutzer, preprint) or even sub-grain level as concluded by Kumar et al. (2020).

Another direction to test, for already available multi-grain IR-RF, are fine-grain (polyminerale) mineral fractions. The few attempts reported in the literature yielded promising results (Schilles 2002; Coussot et al., 2019). However, the mixture of minerals in such samples may hamper its application. Meyer et al. (2013) used quantitative evaluation of minerals by scanning electron microscopy (QEMSCAN) for polyminerale fine grain OSL samples from interglacial lacustrine units (NW11 and THG 4 from Switzerland; Lowick et al., 2012) and found that K-feldspar amounts only to ~2–4 %. The major component of the samples was quartz (40–50 %). Tsukamoto et al. (2012) confirmed similar observations for various loess samples using X-ray diffractometry (XRD) as well as scanning electron microscopy-energy dispersive X-ray (SEM-EDX). While quartz samples emit RF in the IR region, but not beyond 735 nm (Schmidt et al., 2015), quartz may not interfere with the main IR-RF emission (865 nm). However, the polyminerale composition may lead to unfortunate emission spectra with, e.g., a dominating peak at 710 nm (cf. Heydari et al., 2021, for an unsuccessful IR-RF dating attempt using polyminerals). Hence, for such an application, spectrometer measurements appear indispensable. Besides, deploying IR-RF on polyminerale fine grain samples would significantly broaden the application to environmental settings where grain sizes <90 µm dominate, and applications can be tested preferably without extensive methodological research.

In summary, the current status of IR-RF dating still leaves room for rich methodological and application studies towards a potentially bright future.

Acknowledgements

We are grateful to Sébastien Huot, Frank Preusser and two anonymous reviewers for their patience, constructive comments, and strong support for this manuscript. M.K. Murari and M. Fuchs were supported by the German Research Foundation (DFG FU417/19-1). S. Kreutzer and N. Mercier received financial support by the LaScArBx. LaScArBx is a research programme supported by the ANR (ANR-10-LABX-52). The contribution of S. Kreutzer in 2020 received funding from the European Union's Horizon 2020 research and innovation programme under the Marie

1010 Skłodowska-Curie grant agreement No 844457 (CREDit). M. Frouin was supported by the John
1011 Fell Fund (161/067 and 171/006) University of Oxford. N. Klasen received funding by the
1012 Deutsche Forschungsgemeinschaft (DFG, German Research Foundation) – Project number
1013 57444011 – CRC 806 "Our way to Europe ". All authors thank L. Diehl for drawing Figure 3.

1014

Figure captions

Figure 1

Schematic of the different luminescence transitions involved in IR-RF, IRSL and post-IR IRSL measurements, based on Trautmann et al. (1998, 1999a, 2000a) and Jain and Ankjærgaard (2011). Colours read as follows: Black lines indicate electron transitions; blue lines indicate hole migrations. Red colours also refer to electron transitions but related to the production of IRSL. [a] Exposure to ionizing radiation results in a constant flux of electrons from the valence band to the conduction band. These electrons may recombine radiatively [b], non-radiatively (not-shown for clarity), drop immediately back to the valence band (not-shown for clarity) or populate the IRSL trap [c]. Electrons that populate the IRSL trap pass through the excited state, resulting in infrared radiofluorescence (1.43 eV). Electrons within the IRSL trap are sensitive to infrared light and preferentially recombine with proximal holes. Additionally, the electrons may tunnel directly from the ground-state of the trap [d] (anomalous fading). Alternatively, Trautmann (2000) and Trautmann et al. (2000a) proposed hole production by allowing a direct transition of electrons into the valence band. This facilitates new possibilities for the recombination of electrons in the IRSL trap [e]. Note that each electron stimulated from the valence band will result in the production of a hole. However, these are not shown for clarity. If the electrons are stimulated with infrared light, they reach the excited state of the trap, from which they can migrate locally [f] before recombining. Higher temperature stimulations provide phonon-assistance (dashed black arrows), allowing post-IR IRSL signals to be measured from electrons that have diffused through the band-tail states to more distal holes [g], which are thermally and athermally more stable.

Figure 2

Schematic representation of self-made and commercially available measurement devices. A) The device used by Erfurt (redrawn after Erfurt et al., 2003). B) The device used by Schilles (redrawn after Schilles, 2002). C) The device manufactured by *Risø* laboratories (redrawn after Lapp et al., 2012). D) The device manufactured by Freiberg Instruments (redrawn after Richter et al., 2013)

Figure 3

The efficiencies of four different spectrometers. The overall efficiencies of spectrometers were approximated by multiplying the individual efficiencies of the grating with those of the spectrograph and the CCD chip.

Figure 4

Effective detection band for (A) the setups used by Schilles (2002) and Erfurt (2003b), and (B) *Risø* and *lexsyg research* readers. The net transitions were estimated by interpolation and by multiplying the filter transmission and quantum efficiency of the PMT.

Figure 5

Simulated Gaussian IR-RF peaks from K-feldspar at 710 nm, 865 nm and 910 nm (similar to Erfurt and Krbetschek, 2003b). The main IR-RF peak is centred at 865 nm. A) Simulated IR-RF spectrum with a high 865 nm peak, simulating a bleached sample. B) Simulated IR-RF spectrum with a high 710 nm peak, a situation appearing when the sample is dosed. C) A typical spectrum from K-feldspar for a sediment sample (redrawn after Schilles, 2002).

Figure 6

IR-RF bleaching using different bleaching sources. A) Sunlight bleaching (redrawn after Trautmann et al., 1999a). Full signal resetting is reached within 4–6 h. B) Monochromatic bleaching for wavelengths <500 nm; a bleaching plateau seems to be reached within ca. 0.3 h (redrawn after Trautmann et al., 2000a). C) Solar simulator (200 W high-pressure Hg-lamp, 5 mm Schott KG3 heat absorbing filter at a distance 20 cm) allows full signal resetting within 0.7 h (redrawn after Krbetschek et al., 2000). D) A bleaching comparison of IR-RF measured at elevated temperature (RF₇₀) with IR₅₀, pIRIR₂₂₅ and pIRIR₂₉₀ (redrawn after Frouin et al., 2017). Resetting of the IR-RF signal is much slower compared to IR₅₀ and pIRIR₂₂₅, but it is similar or slightly faster than pIRIR₂₉₀ and needs ~3 h bleaching time. The x-axis scale is similar for all subplots.

Figure 7

IR phosphorescence of a K-feldspar sample after bleaching as observed by Erfurt and Krbetschek (2003b) (redrawn after Erfurt and Krbetschek, 2003b).

Figure 8

A schematic representation to explain the sensitivity change monitored by various authors using different methods. A) Derived sensitivity correction factor (s) by fitting exponential functions to two bleached regenerated IR-RF (RF_{reg}) curves (Schilles, 2002). B) Sensitivity correction factor (F_s) estimation using spline fitting and extrapolation (Varma et al., 2013). C) Sensitivity correction of IR-RF data by sliding the natural IR-RF (RF_{nat}) curve vertically up or down along with horizontal sliding to find the best match with the RF_{reg} curve (see main text for detail).

Figure 9

A) A typical behaviour of the initial rise of IR-RF from a natural sample. The first few channels of the measured data show an initial rise in IR-RF intensity before decaying monotonically. B) IR-RF signal dynamic range measured while irradiating the sample with a cumulative dose of 3,900 Gy. The typical dynamic range of IR-RF signals is ~ 2 , as reported by Schilles (2002) and (Erfurt, 2003b).

Figure 10

IR-RF signal stability with respect to pulse annealing temperature. A) All natural IR-RF (RF_{nat}) signals measured for a fixed short duration at different annealing temperatures. All samples show an increase in IR-RF up to 150 °C. For samples Gro8 and Es1 the signal decrease for temperatures > 250 °C, but remains stable for sample Ook1, a > 1 Ma old sample (redrawn after Trautmann et al., 1999a). B) The signal remains stable until ca 250 °C for RF_{nat} and regenerated IR-RF (RF_{reg}) for sample TH8 and changes its intensity for temperatures > 250 °C (redrawn after Frouin et al., 2017).

Figure 11

Graphical representation of IR-RF data analysis techniques used to determine the D_e . A) The D_e is obtained by extrapolation using the fitted natural IR-RF signal. B) The natural IR-RF signal is used to re-calculate the D_e using the fitted regenerated IR-RF curve after bleaching. C) The natural and the regenerated IR-RF signals are recorded before both are matched via (horizontal) sliding. D) The natural curve is moved up or down via vertically sliding to find both curves' best match. The D_e is defined as the offset of the natural signal on the x-axis (for further details, see main text).

Figure 12

Simulated IR-RF curves for different equations reported in the literature, with Φ_0 the initial IR-RF photon flux, $\Delta\Phi$ the dose-dependent change of the IR-RF flux, λ the decay parameter, β the dispersion factor and D the dose. For similar parameter values, the curve shapes differ markedly. Values chosen for the figure: $\Phi_0 = 1$, $\Delta\Phi = 1$, $\lambda = 2.274\text{e-}03$, $\beta = 7.6\text{e-}01$.

Figure 13

A) Independent age control vs IR-RF age (redrawn after Degering and Krbetschek, 2007). All IR-RF ages match within the error limits when compared to independent ages. B) All IR-RF ages show either over or underestimation compared to independent age control (redrawn from supplement data, Buylaert et al., 2012). C) Independent age control vs IR-RF ages measured with a modified IRSAR protocol (RF₇₀) (redrawn after Frouin et al., 2017). Almost all ages match within 2σ uncertainty. Abbreviations used in figure legends: IR-RF SOL2: IR-RF ages when samples are bleached for 4 h using the external solar lamp Hönle SOL2, Biost.: Biostratigraphy, IRSL-50_{fc}: Fading corrected IRSL age.

Table captions

Table 1: The main emission bands and possible defects observed in feldspar (copyright by Prasad 2017, permission granted by the author).

Table 2: Irradiation source parameters for various devices used for IR-RF stimulation.

Table 3: The relevant parameters for different spectrometer configurations.

Table 4: Detection parameters for various devices used for IR-RF detection.

Table 5: Bleaching source parameters for various devices used for IR-RF bleaching.

Table 6: Overview of published IR-RF measurement protocols used for D_e determination.

Table 1:

<i>Emission band</i>	<i>Excitation</i>	<i>Possible origin</i>	<i>Reference</i>
~3.8–4.4 eV (280–320 nm)	TL	Strain and/or ionic diffusion	Garcia-Guinea et al. (1999)
	PL	Tl ⁺	Gorobets et al. (1995)
	IRSL		Baril and Huntley (2003a)
	TR-OSL		Clark and Bailiff (1998)
~3.1 eV (400 nm)	CL	Paramagnetic defect	*Finch and Klein (1999)
	IRSL	?	Rieser et al. (1999)
	IRSL	?	Baril and Huntley (2003a)
~2.2 eV (560 nm)	IRSL	Mn ²⁺	Rieser et al. (1997)
	IRSL		Baril and Huntley (2003a)
	CL		Geake et al. (1977)
	TR-OSL		Clark and Bailiff (1998)
~1.7 eV (730 nm)	Absorption	Fe ³⁺	White et al. (1986)
	PL		Telfer and Walker (1975)
	IRSL		Krbetschek et al. (1997)
	PL		Poolton et al. (1996, 2006)
~1.45 eV (855 nm)	RL or RF	IRSL dating trap	Trautmann et al. (1998)
~1.41–1.3 eV (900 nm) (~880 nm and ~955 nm)	CL (at 7 K)	IRCL trap with two sites and Fe ⁴⁺ as a competitor	Kumar et al. (2020)
~1.3–1.36 eV (910 nm)	RL or RF	Pb ⁺	Erfurt (2003b)
	Post IR phosphorescence	IRSL dating trap	Baril and Huntley (2003a)
	TL	?	Krbetschek and Rieser (1995)

TL: Thermoluminescence, IRSL: Infrared stimulated luminescence, CL: Cathodoluminescence, RF: Radiofluorescence, RL: Radioluminescence, PL: Photoluminescence

TR-OSL: Time-resolved optically stimulated luminescence, IRCL: Infrared Cathodoluminescence

* Finch and Klein (1999) reported the peak maximum at 430 nm related to Al³⁺-O²⁻-Al³⁺ “Löwenstein” bridges.

Table 2:

<i>Laboratory / Manufacturer</i>	<i>Radiation source</i>	<i>Activity [GBq]</i>	<i>Radiation Type</i>	<i>Source type</i>	<i>Dose rate [Gy min⁻¹]</i>	<i>Active area [mm²]</i>	<i>Reference</i>
Freiberg	¹³⁷ Cs/ ¹³⁷ Ba	0.0037	β and γ	Planar	0.050	19.6	Trautmann (1999)
Freiberg	¹³⁷ Cs/ ¹³⁷ Ba	0.0050	β and γ	Planar	0.080	50.3	Erfurt (2003b)
Heidelberg	¹³⁷ Cs/ ¹³⁷ Ba	0.0037	β and γ	Planar	0.034	28.3	Schilles (2002)
Risø	⁹⁰ Sr/ ⁹⁰ Y	1.48	β	Planar	2.640	50.3	Buylaert et al. (2012)
Freiberg Instruments	⁹⁰ Sr/ ⁹⁰ Y	1.6–2	β	Ring	2.250	n.a.	Richter et al. (2012)

Erfurt calibrated the radiation source with Al₂O₃:C while the other readers were calibrated with natural (calibration) quartz.

Table 3:

<i>Laboratory / Manufacturer</i>	Spectrograph	<i>Spectrograph/Grating</i>		Dispersion [nm]	Company	<i>CCD Camera</i>			<i>Reference</i>
		Grating	Blazed			Camera type	Active Pixels	Cooling Type	
Freiberg	Jobin Yvon CP200	Holographic	Not applicable	300–1000	Marconi	NA	1152x298	-100 °C (Liquid nitrogen)	Rieser et al. (1994)
Freiberg	Jobin-Yvon CP200	Holographic	Not applicable	250–1152	Marconi	Front-illuminated	1152x352	-100 °C (Liquid nitrogen)	Erfurt (2003b), Rieser et al. (1994)
Heidelberg	Acton SP150	150 lines/mm	300 nm	200–1100	Princeton Instruments	Back-illuminated	1100x330	-100 °C (Liquid nitrogen)	Rieser et al. (1999)
Freiberg Instruments	Andor Shamrock 163	300 lines/mm	500 nm	200–1050	Andor Newton 920-BU/iDus 420 OE	Back-illuminated / Open Electrode	1024x255	-80 °C (TE Cooled)	Richter et al. (2013)

TE Cooled: Thermoelectric cooling

Table 4:

Laboratory/ Manufacturer	Detector	Detection [nm]	Filters	Bandpass [nm]	Light collection	References
Freiberg	Spectrometer	300–1000	No filter	300-1000	Optical Guide	*Trautmann (1999)
Freiberg	Spectrometer / Hamamatsu (R943-02)	160–930	HQ865/20	855-875	Optical Guide	#Erfurt (2003b)
Heidelberg	Spectrometer / Hamamatsu (R943-02)	160–930	IR83 HOYA	820-930	Optical Guide	#Schilles (2002)
Risø	Hamamatsu (H7421-50)	380–890	Chroma D900/100	850-890	Optical Guide	Buylaert et al. (2012)
Freiberg Instruments	Spectrometer / Hamamatsu (H7421-50)	380–890	Chroma D850/40	845-885	Direct	Richter et al. (2013)

*Trautmann's research was based on spectrometer measurements using a 200–800 nm detection range. Later, the spectrometer was modified for detecting 300–1,000 nm. The integrated counts of IR-RF peak were used to estimate the D_e .

#Schilles and Erfurt used liquid-cooled thermoelectric housing (LCT50, Thorn EMI) at about -20 °C to reduce the thermal noise.

Table 5:

<i>Laboratory/ Manufacturer</i>	<i>Bleaching source</i>	<i>Spectrum</i>	<i>Max Power*</i> <i>[mW cm⁻²]</i>	<i>Connection</i>	<i>Reference</i>
Freiberg	Hg-Lamp	UV-VIS	--	Optical Guide	[#] Trautmann (1999)
Freiberg	250W OSRAM LAMP	UV-VIS	100	Optical Guide	[†] Erfurt (2003b)
Heidelberg	150W QTH	UV-VIS	80	Optical Guide	[†] Schilles (2002)
Risø	UV LED	UV	700	Direct	Buylaert et al. (2012)
Freiberg Instruments	6 LED solar simulator	UV-IR	700	Direct	Richter et al. (2013)

*Maximum power density of the bleaching units refers to approximate power at the sample position. It can vary from device to device.

[#]Trautmann (1999) used an interference filter in front of the solar lamp for monochromatic bleaching.

[†]Schilles (2002) and Erfurt (2003b) both used an IR cut-off filter.

1 Table 6:

Reference	Protocol Abbr.	Treatments and observations ¹						Data analysis	Comments
		#1	#2	#3	#4	#5	#6		
Buylaert et al. (2012)	NA (based on IRSAR)	-	IR-RF [RF_{nat}]	Bleaching ($\geq 1,800$ s) (ca. 395 nm)	Pause ($\geq 3,600$ s)	-	IR-RF [RF_{reg}]	Sliding	-
Erfurt and Krbetschek (2003b)	IRSAR	-	IR-RF [RF_{nat}]	Bleaching ($\geq 1,800$ s) (artificial solar spectrum)	Pause ($\geq 3,600$ s)	-	IR-RF [RF_{reg}]	Fitting (interp.)	RF_{nat} is represented by only a few channels
Frouin et al. (2017)	RF ₇₀ (based on IRSAR)	PH@70 °C (900 s)	IR-RF@70 °C [RF_{nat}]	Bleaching@70 °C ($\geq 7,200$ s) (artificial solar spectrum)	Pause ($\geq 3,600$ s)	PH@70 °C (900 s)	IR-RF@70 °C [RF_{reg}]	Sliding	-
Krbetschek et al. (2000)	NA	-	IR-RF [RF_{nat}]	Bleaching ($\geq 1,800$ s) (artificial solar spectrum)	-	-	IR-RF [RF_{reg}]	Fitting Sliding	Based on the results by Trautmann et al. (1999a), but with artificial bleaching
Trautmann et al. (1999a)	NA	-	IR-RF [RF_{nat}]	Bleaching (natural sunlight)	-	-	IR-RF [RF_{reg}]	Fitting (extrapol.)	RF_{reg} is represented by only a few channels
Schilles (2002)	NA	-	IR-RF [RF_{nat}]	Bleaching $\geq 3,600$ s) (artificial solar spectrum)	Pause ($\geq 1,800$ s)	-	IR-RF [RF_{reg}]	Fitting	Combination of extrapolation and interpolation for the data analysis; sensitivity correction using a separate aliquot (Schilles, 2002, p. 97)
Varma et al. (2013) ²	NA (based on IRSAR)	-	IR-RF [RF_{nat}]	Bleaching (≥ 800 s) (ca. 395 nm)	-	-	IR-RF [RF_{reg}]	Sliding	200 s phosphorescence measurement before and after each IR-RF measurement; Repeat step #3 and #6 to monitor sensitivity changes

¹The instrumental setup differs considerably across the studies and should be considered before protocol application. If no measurement temperature is listed, such value was not reported by the study or no additional heating above ambient temperature was applied. Please note that the table lists only general treatments, for further details the reader is referred to the respective publication.

²The authors used their protocol for dose recovery tests only; distinct D_e determinations are not mentioned.

PH: Preheat | NA: Not available

9 **References**

- 10 Aitken, M.J., 1985a. Thermoluminescence dating. Academic Press.
- 11 Aitken, M.J., 1985b. Alpha particle effectiveness: numerical relationship between systems.
12 Ancient TL 3, 22–25.
- 13 Aitken, M.J., 1998. An introduction to optical dating. Oxford University Press.
- 14 Auclair, M., Lamothe, M., Huot, S., 2003. Measurement of anomalous fading for feldspar IRSL
15 using SAR. Radiation Measurements 37, 487–492. doi:10.1016/S1350-4487(03)00018-0
- 16 ASTM International, 2012. ASTM G173-03(2012) Standard Tables for Reference Solar Spectral
17 Irradiances: Direct Normal and Hemispherical on 37° Tilted Surface, ASTM International,
18 West Conshohocken, PA. <http://www.astm.org>. doi: 10.1520/G0173-03R12
- 19 Baril, M.R., Huntley, D.J., 2003a. Optical excitation spectra of trapped electrons in irradiated
20 feldspars. J. Phys.: Condens. Matter 15, 8011–8027. doi: 10.1088/0953-8984/15/46/017.
- 21 Baril, M.R., Huntley, D.J., 2003b. Infrared stimulated luminescence and phosphorescence spectra
22 of irradiated feldspars. J. Phys.: Condens. Matter 15, 8029–8048. doi: 10.1088/0953-
23 8984/15/46/018.
- 24 Baumann, W., Mania, D., Toepfer, V., Eißmann, L., 1983. Die paläolithischen Neufunde von
25 Markkleeberg bei Leipzig. Landesmuseum für Vorgeschichte Dresden 16.
- 26 Brooks, R.J., Finch, A.A., Hole, D.E., Townsend, P.D., Wu, Z.-L., 2002. The red to near-infrared
27 luminescence in alkali feldspar. Contributions to Mineralogy and Petrology 143, 484–494.
28 doi: 10.1007/s00410-002-0359-4.
- 29 Buylaert, J.P., Jain, M., Murray, A.S., Thomsen, K.J., Lapp, T., 2012. IR-RF dating of sand-sized
30 K-feldspar extracts: A test of accuracy. Radiation Measurements 47, 759–765. doi:
31 10.1016/j.radmeas.2012.06.021.
- 32 Buylaert, J.P., Murray, A.S., Thomsen, K.J., Jain, M., 2009. Testing the potential of an elevated
33 temperature IRSL signal from K-feldspar. Radiation Measurements 44, 560–565. doi:
34 10.1016/j.radmeas.2009.02.007.

- Clark, R.J., Bailiff, I.K., 1998. Fast time-resolved luminescence emission spectroscopy in some feldspars. *Radiation Measurements* 29, 553–560. doi: 10.1016/S1350-4487(98)00068-7.
- Coussot, C., Liard, M., Kreutzer, S., Mercier, N., 2019. Séquence de Comblement d'un Paléovallon en Contexte de Plateau (290-10 Ka) : La Coupe De Courville-Sur-Eure (Eure-Et-Loir, France). *Quaternaire*, 167–183.
- Degering, D., Krbetschek, M.R., 2007. Dating of interglacial sediments by luminescence methods, in: *The climate of past interglacials. Developments in Quaternary Sciences*. Elsevier, pp. 157–171. doi: 10.1016/S1571-0866(07)80036-4.
- Duller, G.A.T., 1992. Luminescence chronology of raised marine terraces, South-West North Island, New Zealand. PhD thesis, University of Aberystwyth, UK, pp. 236.
- Efron, B., 1979. Bootstrap Methods: Another Look at the Jackknife. *Ann. Statist.* 7, 1–26. doi: 10.1214/aos/1176344552.
- Eissmann, L., 2002. Quaternary geology of eastern Germany (Saxony, Saxon-Anhalt, South Brandenburg, Thuringia), type area of the Elsterian and Saalian Stages in Europe. *Quaternary Science Reviews* 21, 1275-1346. doi: 10.1016/S0277-3791(01)00075-0.
- Erfurt, G., 2003a. Infrared luminescence of Pb^{+} centres in potassium-rich feldspars. *Physica status solidi (a)* 200, 429–438. doi: 10.1002/pssa.200306700.
- Erfurt, G., 2003b. Radiolumineszenzspektroskopie und -dosimetrie an Feldspäten und synthetischen Luminophoren für die geochronometrische Anwendung. PhD thesis, Technische Universität Bergakademie Freiberg, Germany, pp. 141.
- Erfurt, G., Krbetschek, M.R., 2003a. Studies on the physics of the infrared radioluminescence of potassium feldspar and on the methodology of its application to sediment dating. *Radiation Measurements* 37, 505–510. doi: 10.1016/S1350-4487(03)00058-1.
- Erfurt, G., Krbetschek, M.R., 2003b. IRSAR - A single-aliquot regenerative-dose dating protocol applied to the infrared radiofluorescence (IR-RF) of coarse-grain K-feldspar. *Ancient TL* 21, 35–42.

- Erfurt, G., Krbetschek, M.R., Bortolot, V.J., Preusser, F., 2003. A fully automated multi-spectral radioluminescence reading system for geochronometry and dosimetry. *Nuclear Instruments and Methods in Physics Research Section B: Beam Interactions with Materials and Atoms* 207, 487–499. doi: 10.1016/S0168-583X(03)01121-2.
- Finch, A.A., Klein, J., 1999. The causes and petrological significance of cathodoluminescence emissions from alkali feldspars. *Contributions to Mineralogy and Petrology* 135, 234–243. doi: 10.1007/s004100050509.
- Frouin, M., 2014. Les feldspaths comme support pour la datation par luminescence de gisements archéologiques et de séquences quaternaires d'Aquitaine. PhD thesis, Université Bordeaux Montaigne, France, pp. 390.
- Frouin, M., Huot, S., Kreutzer, S., Lahaye, C., Lamothe, M., Philippe, A., Mercier, N., 2017. An improved radiofluorescence single-aliquot regenerative dose protocol for K-feldspars. *Quaternary Geochronology* 38, 13–24. doi: 10.1016/j.quageo.2016.11.004.
- Frouin, M., Huot, S., Mercier, N., Lahaye, C., Lamothe, M., 2015. The issue of laboratory bleaching in the infrared-radiofluorescence dating method. *Radiation Measurements* 81, 212–217. doi: 10.1016/j.radmeas.2014.12.012.
- Fu, X., Zhang, J.-F., Zhou, L.-P., 2012. Comparison of the properties of various optically stimulated luminescence signals from potassium feldspar. *Radiation Measurements* 47, 210–218. doi:10.1016/j.radmeas.2011.12.007
- Garcia-Guinea, J., Townsend, P.D., Sanchez-Muñoz, L., Rojo, J.M., 1999. Ultraviolet-blue ionic luminescence of alkali feldspars from bulk and interfaces. *Physics and Chemistry of Minerals* 26, 658–667. doi: 10.1007/s002690050231.
- Geake, J.E., Walker, G., Telfer, D.J., Mills, A.A., 1977. The cause and significance of luminescence in lunar plagioclase. *Philosophical Transactions of the Royal Society A: Mathematical, Physical and Engineering Sciences* 285, 403–408. doi: 10.1098/rsta.1977.0081.

- Gorobets, B.S., Portnov, A.M., Rogozhin, A.A., 1995. Luminescence spectroscopy of the earth. *Radiation Measurements* 24, 485–491. doi: 10.1016/1350-4487(94)00124-J.
- Guérin, G., Valladas, G., 1980. Thermoluminescence dating of volcanic plagioclases. *Nature* 286, 697–699. doi: 10.1038/286697a0.
- Herber, L.J., 1969. Separation of Feldspar from Quartz by Flotation. *The American Mineralogist* 54, 1212–1215.
- Hetzel, R., Tao, M., Niedermann, S., Strecker, M.R., Ivy-Ochs, S., Kubik, P.W., Gao, B., 2004. Implications of the fault scaling law for the growth of topography: mountain ranges in the broken foreland of north-east Tibet. *Terra Nova* 16, 157–162. doi:10.1111/j.1365-3121.2004.00549.x
- Heydari, M., Guérin, G., Zeidi, M., Conard, N. J., 2021. Bayesian luminescence dating at Ghār-e Boof, Iran, provides a new chronology for Middle and Upper Paleolithic in the southern Zagro. *Journal of Human Evolution* 151, 102926. doi:10.1016/j.jhevol.2020.102926
- Huntley, D.J., 2006. An explanation of the power-law decay of luminescence. *J. Phys.: Condens. Matter* 18, 1359–1365. doi: 10.1088/0953-8984/18/4/020.
- Huntley, D.J., Godfrey-Smith, D., Thewalt, M., 1985. Optical dating of sediments. *Nature* 313, 27–33. <https://doi.org/10.1038/313105a0>.
- Huntley, D.J., Lamothe, M., 2001. Ubiquity of anomalous fading in K-feldspars and the measurement and correction for it in optical dating. *Canadian Journal of Earth Sciences* 38, 1093–1106. doi: 10.1139/cjes-38-7-1093.
- Huntley, D.J., Lian, O.B., 2006. Some observations on tunnelling of trapped electrons in feldspars and their implications for optical dating. *Quaternary Science Reviews* 25, 2503–2512. doi: [10.1016/j.quascirev.2005.05.011](https://doi.org/10.1016/j.quascirev.2005.05.011).
- Hütt, G., Jaek, I., Tchonka, J., 1988. Optical dating: K-Feldspars optical response stimulation spectra. *Quaternary Science Reviews* 7, 381–385. doi: 10.1016/0277-3791(88)90033-9.

- Huot, S., Frouin, M., Lamothe, M., 2015. Evidence of shallow TL peak contributions in infrared radiofluorescence. *Radiation Measurements* 81, 237–241. doi: 10.1016/j.radmeas.2015.05.009.
- Jain, M., Ankjærgaard, C., 2011. Towards a non-fading signal in feldspar: Insight into charge transport and tunnelling from time-resolved optically stimulated luminescence. *Radiation Measurements* 46, 292–309. doi: 10.1016/j.radmeas.2010.12.004.
- Kadereit, A., Kühn, P., Wagner, G.A., 2010. Holocene relief and soil changes in loess-covered areas of south-western Germany: The pedosedimentary archives of Bretten-Bauerbach (Kraichgau). *Quaternary International* 222, 96–119. doi: 10.1016/j.quaint.2009.06.025.
- Kars, R.H., Wallinga, J., 2009. IRSL dating of K-feldspars: Modelling natural dose response curves to deal with anomalous fading and trap competition. *Radiation Measurements* 44, 594–599.
- Klasens, H.A., 1946. Transfer of energy between centres in zinc sulphide phosphors. *Nature* 158, 306–307. doi: 10.1038/158306c0.
- Krbetschek, M.R., Götze, J., Irmer, G., Rieser, U., Trautmann, T., 2002. The red luminescence emission of feldspar and its wavelength dependence on K, Na, Ca \pm composition. *Mineralogy and Petrology* 76, 167–177. doi:10.1007/s007100200039
- Krbetschek, M.R., Degering, D., Alexowsky, W., 2008. Infrarot-Radiofluoreszenz-Alter (IR-RF) unter-saalezeitlicher Sedimente Mittel- und Ostdeutschlands. *Zeitschrift der Deutschen Gesellschaft für Geowissenschaften* 159, 133–140. doi: 10.1127/1860-1804/2008/0159-0133.
- Krbetschek, M.R., Götze, J.U., Dietrich, A., Trautmann, T., 1997. Spectral information from minerals relevant for luminescence dating. *Radiation Measurements* 27, 695–748. doi: 10.1016/S1350-4487(97)00223-0.
- Krbetschek, M.R., Rieser, U., 1995. Luminescence spectra of alkali feldspars and plagioclases. *Radiation Measurements* 24, 473–477. doi: 10.1016/1350-4487(95)00011-3.

- Krbetschek, M.R., Trautmann, T., 2000. A spectral radioluminescence study for dating and dosimetry. *Radiation Measurements* 32, 853–857. doi: 10.1016/S1350-4487(00)00085-8.
- Krbetschek, M.R., Trautmann, T., Dietrich, A., Stolz, W., 2000. Radioluminescence dating of sediments: methodological aspects. *Radiation Measurements* 32, 493–498. doi: 10.1016/S1350-4487(00)00122-0.
- Krbetschek, M.R., Erfurt, G., Degering, D. 2003. *Radiofluorescence dating*: A novel method for age determination of clastic sediment deposits from about 20 ka to 300 ka. Poster presentation; XVI Inqua Congress, Reno (USA).
- Kreutzer, S., Duval, M., Bartz, M., Bertran, P., Bosq, M., Eynaud, F., Verdin, F., Mercier, N., 2018a. Deciphering long-term coastal dynamics using IR-RF and ESR dating: A case study from Médoc, south-west France. *Quaternary Geochronology* 48, 108–120. doi: 10.1016/j.quageo.2018.09.005.
- Kreutzer, S., Lauer, T., Meszner, S., Krbetschek, M.R., Faust, D., Fuchs, M., 2014. Chronology of the Quaternary profile Zeuchfeld in Saxony-Anhalt / Germany – a preliminary luminescence dating study. *Zeitschrift für Geomorphologie* 58, 5–26. doi: 10.1127/0372-8854/2012/S-00112.
- Kreutzer, S., Martin, L., Dubernet, S., Mercier, N., 2018b. The IR-RF alpha-Efficiency of K-feldspar. *Radiation Measurements* 120, 148–156. doi: 10.1016/j.radmeas.2018.04.019.
- Kreutzer, S., Burow, C., Dietze, M., Fuchs, M., Schmidt, C., Fischer, M., Friedrich, J., 2018c. Luminescence: Comprehensive Luminescence Dating Data Analysis. R package version 0.8.6, <https://CRAN.R-project.org/package=Luminescence>.
- Kreutzer, S., Murari, M.K., Frouin, M., Fuchs, M., Mercier, N., 2017. Always remain suspicious: a case study on tracking down a technical artefact while measuring IR-RF. *Ancient TL* 35, 20–30.
- Kreutzer, S., Schmidt, C., Fuchs, M.C., Dietze, M., Fischer, M., Fuchs, M., 2012. Introducing an R package for luminescence dating analysis. *Ancient TL* 30, 1–8.

- Kumar, R., Kook, M., Murray, A.S., Jain, M., 2018. Towards direct measurement of electrons in metastable states in K-feldspar: Do infrared-photoluminescence and radioluminescence probe the same trap? *Radiation Measurements* 120, 1–17. doi: [10.1016/j.radmeas.2018.06.018](https://doi.org/10.1016/j.radmeas.2018.06.018).
- Kumar, R., Martin, L.I.D.J., Poelman, D., Vandenberghe, D., De Grave, J., Kook, M., Jain, M., 2020. Site-selective mapping of metastable states using electron-beam induced luminescence microscopy. *Sci Rep* 10, 1270–14. doi:10.1038/s41598-020-72334-7
- Kumar, R., Kook, M., Jain, M., 2021. Sediment dating using Infrared Photoluminescence. *Quaternary Geochronology* 62, 101147. doi:10.1016/j.quageo.2020.101147
- Lamothe, M., Auclair, M., Hamzaoui, C., Huot, S., 2003. Towards a prediction of long-term anomalous fading of feldspar IRSL. *Radiation Measurements* 37, 493–498.
- Lamothe, M., Brisson, L.F., Hardy, F., 2020. Circumvention of anomalous fading in feldspar luminescence dating using Post-Isothermal IRSL. *Quaternary Geochronology* 57, 101062. doi:10.1016/j.quageo.2020.101062
- Larsen, E., Johannessen, N.E., Kowalczyk, P.B., Kleiv, R.A., 2019. Selective flotation of K-feldspar from Na-feldspar in alkaline environment. *Minerals Engineering* 142, 105928. doi:10.1016/j.mineng.2019.105928
- Lapp, T., Jain, M., Thomsen, K.J., Murray, A.S., Buylaert, J.P., 2012. New luminescence measurement facilities in retrospective dosimetry. *Radiation Measurements* 47, 803–808. doi: 10.1016/j.radmeas.2012.02.006
- Lauer, T., Krbetschek, M.R., Frechen, M., Tsukamoto, S., Hoselmann, C., Weidenfeller, M., 2011. Infrared radiofluorescence (IR-RF) dating of middle pleistocene fluvial archives of the Heidelberg Basin (Southwest Germany). *Geochronometria* 38, 23–33. doi: 10.2478/s13386-011-0006-9.
- Lauer, T., Weiss, M., 2018. Timing of the Saalian- and Elsterian glacial cycles and the implications for Middle – Pleistocene hominin presence in central Europe. *Scientific Reports*, 8: 5111. <https://doi.org/10.1038/s41598-018-23541-w>.

- Li, Y., Tsukamoto, S., Frechen, M., Gabriel, G., 2017. Timing of fluvial sedimentation in the Upper Rhine Graben since the Middle Pleistocene: constraints from quartz and feldspar luminescence dating. *Boreas* 47, 256–270. doi:10.1111/bor.12266
- Li, B., Roberts, R.G., Jacobs, Z., Li, S.-H., 2014. A single-aliquot luminescence dating procedure for K-feldspar based on the dose-dependent MET-pIRIR signal sensitivity. *Quaternary Geochronology* 20, 51–64. doi:10.1016/j.quageo.2013.11.001
- Li, B., Li, S.-H., 2013. The effect of band-tail states on the thermal stability of the infrared stimulated luminescence from K-feldspar. *Journal of Luminescence* 136, 5–10. doi:10.1016/j.jlumin.2012.08.043.
- Li, B., Li, S.-H., 2011a. Luminescence dating of K-feldspar from sediments: A protocol without anomalous fading correction. *Quaternary Geochronology* 6, 468–479. doi:10.1016/j.quageo.2011.05.001.
- Li, B., Li, S.-H., 2011b. Thermal stability of infrared stimulated luminescence of sedimentary K-feldspar. *Radiation Measurements* 46, 29–36. doi:10.1016/j.radmeas.2010.10.002
- Liu, J., Murray, A.S., Buylaert, J.-P., Jain, M., Chen, J., Lu, Y., 2016. Stability of fine-grained TT-OSL and post-IR IRSL signals from a c. 1 Ma sequence of aeolian and lacustrine deposits from the Nihewan Basin (northern China). *Boreas* 45, 703–714. doi:10.1111/bor.12180
- Lowick, S.E., Trauerstein, M., Preusser, F., 2012. Testing the application of post IR-IRSL dating to fine grain waterlain sediments. *Quaternary Geochronology* 8, 33–40. doi:10.1016/j.quageo.2011.12.003.
- Lowick, S.E., Valla, P.G., 2018. Characterising the luminescence behaviour of 'infinitely old' quartz samples from Switzerland. *Quaternary Geochronology* 43, 1–11. doi:10.1016/j.quageo.2017.09.004.
- Marfunin, A.S., Bershov, L.V., 1970. Paramagnetic in feldspars and their possible crystalchemical and petrological significance (ПАРАМАГНИТНЫЕ ЦЕНТРЫ В

- 213 ПОЛЕВЫХ ШПАТАХ И ИХ ВОЗМОЖНОЕ КРИСТАЛЛОХИМИЧЕСКОЕ
214 И ПЕТРОГРАФИЧЕСКОЕ ЗНАЧЕНИЕ). Dokl. Akad. Nauk 193, 421–414.
- 215 Marfunin, A.S., 1979. Spectroscopy, luminescence and radiation centers in minerals. Springer
216 Berlin Heidelberg. doi: 10.1007/978-3-642-67112-8.
- 217 Meszner, S., Kreutzer, S., Fuchs, M., Faust, D., 2013. Late Pleistocene landscape dynamics in
218 Saxony, Germany: Paleoenvironmental reconstruction using loess-paleosol sequences.
219 Quaternary International 296, 95–107. doi: 10.1016/j.quaint.2012.12.040.
- 220 Meyer, M.C., Austin, P., Tropper, P., 2013. Quantitative evaluation of mineral grains using
221 automated SEM–EDS analysis and its application potential in optically stimulated
222 luminescence dating. Radiation Measurements 58, 1–11. doi: 10.1016/j.radmeas.2013.07.004.
- 223 Miallier, D., Sanzelle, S., Fain, J., 1983. The use of flotation technique to separate quartz from
224 feldspar. Ancient TL 5–6.
- 225 Mittelstrass, D., Kreutzer, S., preprint. Spatially Resolved Infrared Radiofluorescence: Single-
226 grain K-feldspar Dating using CCD Imaging, Geochronology Discussion, 1-31. doi:
227 10.5194/gchron-2020-43
- 228 Murari, M.K., Kreutzer, S., Fuchs, M., 2018. Further investigations on IR-RF: Dose recovery and
229 correction. Radiation Measurements 120, 110–119. doi: 10.1016/j.radmeas.2018.04.017.
- 230 Murray, A.S., Buylaert, J.P., Thomsen, K.J., Jain, M., 2009. The effect of preheating on the IRSL
231 signal from feldspar. Radiation Measurements 44, 554–559. doi:
232 10.1016/j.radmeas.2009.02.004.
- 233 Murray, A.S., Wintle, A.G., 2000. Luminescence dating of quartz using an improved single-aliquot
234 regenerative-dose protocol. Radiation Measurements 32, 57–73. doi: 10.1016/S1350-
235 4487(99)00253-X.
- 236 Nagli, L.E., Dyachenko, S.V., 1988. Influence of a v_c -vacancy on luminescence of Pb^+ centres in
237 alkali halides. Phys. stat. sol. (b) 146, 295–301. doi: 10.1002/pssb.2221460131.

- 238 Novothny, Á., Frechen, M., Horváth, E., Krbetschek, M.R., Tsukamoto, S., 2010. Infrared
239 stimulated luminescence and radiofluorescence dating of aeolian sediments from Hungary.
240 Quaternary Geochronology 5, 114–119. doi: 10.1016/j.quageo.2009.05.002.
- 241 Ostrooumov, M., 2016. Amazonite. Elsevier. doi: 10.1016/C2015-0-00152-6.
- 242 Pavesi, L., Ceschini, M., 1993. Stretched-exponential decay of the luminescence in porous silicon.
243 Physical Review B 48, 17625–17628. doi: 10.1103/PhysRevB.48.17625.
- 244 Pagonis, V., Phan, H., Ruth, D., Kitis, G., 2013. Further investigations of tunneling recombination
245 processes in random distributions of defects. Radiation Measurements 58, 66–74.
246 doi:10.1016/j.radmeas.2013.08.006
- 247 Pagonis, V., Kulp, C., 2017. Monte Carlo simulations of tunneling phenomena and nearest
248 neighbor hopping mechanism in feldspars. Journal of Luminescence 181, 114–120.
249 doi:10.1016/j.jlumin.2016.09.014
- 250 Pagonis, V., Friedrich, J., Discher, M., Müller-Kirschbaum, A., Schlosser, V., Kreutzer, S., Chen,
251 R., Schmidt, C., 2019. Excited state luminescence signals from a random distribution of
252 defects: A new Monte Carlo simulation approach for feldspar. Journal of Luminescence 207,
253 266–272. doi:10.1016/j.jlumin.2018.11.024
- 254 Poolton, N.R.J., Bøtter-Jensen, L., Johnsen, O., 1996. On the relationship between luminescence
255 excitation spectra and feldspar mineralogy. Radiation Measurements 26, 93–101. doi:
256 10.1016/1350-4487(95)00288-X.
- 257 Poolton, N.R.J., Bøtter-Jensen, L., Johnsen, O., 1995. Thermo-optical properties of optically
258 stimulated luminescence in feldspars. Radiation Measurements 24, 531–534. doi:
259 10.1016/1350-4487(94)00114-G.
- 260 Poolton, N.R.J., Kars, R.H., Wallinga, J., Bos, A.J.J., 2009. Direct evidence for the participation
261 of band-tails and excited-state tunnelling in the luminescence of irradiated feldspars. J. Phys.:
262 Condens. Matter 21, 485505. doi: 10.1088/0953-8984/21/48/485505.

- Poolton, N.R.J., Mauz, B., Lang, A., Jain, M., Malins, A.E.R., 2006. Optical excitation processes in the near band-edge region of and feldspar. *Radiation Measurements* 41, 542–548. doi: 10.1016/j.radmeas.2005.12.001.
- Poolton, N.R.J., Ozanyan, K.B., Wallinga, J., Murray, A.S., Bøtter-Jensen, L., 2002a. Electrons in feldspar II: a consideration of the influence of conduction band-tail states on luminescence processes. *Physics and Chemistry of Minerals* 29, 217–225. doi: 10.1007/s00269-001-0218-2.
- Poolton, N.R.J., Wallinga, J., Murray, A.S., Bulur, E., Bøtter-Jensen, L., 2002b. Electrons in feldspar I: on the wavefunction of electrons trapped at simple lattice defects. *Physics and Chemistry of Minerals* 29, 210–216. doi: 10.1007/s00269-001-0217-3.
- Porat, N., Faerstein, G., Medialdea, A., Murray, A.S., 2015. Re-examination of common extraction and purification methods of quartz and feldspar for luminescence dating. *Ancient TL* 33, 22–30.
- Prasad, A.K., 2017. Understanding defect related luminescence processes in wide bandgap materials using low temperature multi-spectroscopic techniques. PhD thesis, DTU Nutech, Denmark, pp. 196.
- Prasad, A.K., Jain, M., 2018. Dynamics of the deep red Fe 3+ photoluminescence emission in feldspar. *Journal of Luminescence* 196, 462–469. doi: 10.1016/j.jlumin.2017.11.051.
- Prasad, A.K., Poolton, N.R.J., Kook, M., Jain, M., 2017. Optical dating in a new light: A direct, non-destructive probe of trapped electrons. *Sci Rep* 7, 461. doi: 10.1038/s41598-017-10174-8.
- Preusser, F., Degering, D., Fuchs, M., Hilgers, A., Kadereit, A., Klasen, N., Krbetschek, M.R., Richter, D., Spencer, J.Q.G., 2008. Luminescence dating: basics, methods and applications. *Eiszeitalter und Gegenwart (Quaternary Science Journal)* 57, 95–149. doi: 10.3285/eg.57.1-2.5.

- Prescott, J.R., Huntley, D.J., Hutton, J.T., 1993. Estimation of equivalent dose in thermoluminescence dating - the *Australian slide* method. *Ancient TL* 11, 1–5.
- R Core Team, 2018. R: A Language and Environment for Statistical Computing. R Foundation for Statistical Computing, Vienna, Austria. <https://r-project.org>.
- Qin, J., Chen, J., Li, Y., Zhou, L., 2018. Initial sensitivity change of K-feldspar pIRIR signals due to uncompensated decrease in electron trapping probability: Evidence from radiofluorescence measurements. *Radiation Measurements* 120, 131–136. doi:10.1016/j.radmeas.2018.06.017
- Richter, D., Pintaske, R., Dornich, K., Krbetschek, M.R., 2012. A novel beta source design for uniform irradiation in dosimetric applications. *Ancient TL* 30, 57–63.
- Richter, D., Richter, A., Dornich, K., 2013. lexsyg — a new system for luminescence research. *Geochronometria* 40, 220–228. doi: 10.2478/s13386-013-0110-0.
- Rieser, U., Habermann, J., Wagner, G.A., 1999. Luminescence dating: A new high sensitivity TL/OSL emission spectrometer. *Quaternary Science Reviews* 18, 311–315. doi: 10.1016/S0277-3791(98)00064-X.
- Rieser, U., Hütt, G., Krbetschek, M.R., Stolz, W., 1997. Feldspar IRSL emission spectra at high and low temperatures. *Radiation Measurements* 27, 273–278. doi: 10.1016/S1350-4487(96)00108-4.
- Rieser, U., Krbetschek, M.R., Stolz, W., 1994. CCD-camera based high sensitivity TL/OSL-spectrometer. *Radiation Measurements* 23, 523–528. doi: 10.1016/1350-4487(94)90092-2.
- Scerri, E.M.L., Shipton, C., Clark-Balzan, L., Frouin, M., Schwenninger, J.-L., Groucutt, H.S., Breeze, P.S., Parton, A., Blinkhorn, J., Drake, N.A., Jennings, R., Cuthbertson, P., Omari, A.A., Alsharekh, A.M., Petraglia, M.D., 2018. The expansion of later Acheulean hominins into the Arabian Peninsula. *Scientific Reports* 8, 17165. doi: 10.1038/s41598-018-35242-5.
- Schaarschmidt, M., Fu, X., Li, B., Ben Marwick, Khaing, K., Douka, K., Roberts, R.G., 2019. pIRIR and IR-RF dating of archaeological deposits at Badahlin and Gu Myaung Caves – First luminescence ages for Myanmar. *Quaternary Geochronology* 49, 262–270.

doi:10.1016/j.quageo.2018.01.001

Schäfer, J., Laurat, T., Kegler, J. F., 2003. Bericht zu den Ausgrabungen am altsteinzeitlichen Fundplatz Markkleeberg 1999 bis 2001. Arbeits- und Forschungsberichte zur sächsischen Bodendenkmalpfl. 45, 13–47.

Schilles, T., 2002. Die Infrarot-Radiolumineszenz von Feldspäten und ihr Einsatz in der Lumineszenzdatierung. PhD thesis, Ruprechts-Karls-Universität Heidelberg, Germany, pp. 149.

Schilles, T., Habermann, J., 2000. Radioluminescence dating: the IR emission of feldspar. Radiation Measurements 32, 679–683. doi: 10.1016/S1350-4487(00)00081-0.

Schmidt, C., Kreutzer, S., DeWitt, R., Fuchs, M., 2015. Radiofluorescence of quartz: A review. Quaternary Geochronology 27, 66–77. doi: 10.1016/j.quageo.2015.01.005.

Schön, M., 1942. Zum Leuchtmechanismus der Kristallphosphore. Zeitschrift für Physik 119, 463–471. doi: 10.1007/BF01339783.

Speit, B., Lehmann, G., 1982. Radiation defects in feldspars. Physics and Chemistry of Minerals 8, 77–82. doi: 10.1007/BF00309017.

Spooner, N.A., 1992. Optical dating: Preliminary results on the anomalous fading of luminescence from feldspars. Quaternary Science Reviews 11, 139–145. doi:10.1016/0277-3791(92)90055-D

Sulaymonova, V.A., Fuchs, M.C., Gloaguen, R., Möckel, R., Merchel, S., Rudolph, M., Krbetschek, M.R., 2018. Feldspar flotation as a quartz-purification method in cosmogenic nuclide dating: A case study of fluvial sediments from the Pamir. MethodsX 5, 717–726. doi:10.1016/j.mex.2018.06.014

Telfer, D.J., Walker, G., 1975. Optical detection of Fe³⁺ in lunar plagioclase. Nature 258, 694–695. doi: 10.1038/258694a0.

- Thomsen, K.J., Murray, A.S., Jain, M., Bøtter-Jensen, L., 2008. Laboratory fading rates of various luminescence signals from feldspar-rich sediment extracts. *Radiation Measurements* 43, 1474–1486. doi: 10.1016/j.radmeas.2008.06.002.
- Thomsen, K., Murray, A., Jain, M., 2010. Stability of IRSL signals from sedimentary K-feldspar samples. *Geochronometria* 38, 1–13. doi:10.2478/s13386-011-0003-z
- Toyoda, S., Voinchet, P., Falguères, C., Dolo, J.M., Laurent, M., 2000. Bleaching of ESR signals by the sunlight: a laboratory experiment for establishing the ESR dating of sediments. *Applied Radiation and Isotopes* 52, 1357–1362. doi: 10.1016/S0969-8043(00)00095-6.
- Trautmann, T., 1999. Radiolumineszenzuntersuchungen an Feldspat. PhD thesis, Technische Bergakademie Freiberg, Germany, pp. 99.
- Trautmann, T., 2000. A study of radioluminescence kinetics of natural feldspar dosimeters: experiments and simulations. *Journal of Physics D: Applied Physics* 33, 2304–2310. doi: 10.1088/0022-3727/33/18/315.
- Trautmann, T., Krbetschek, M.R., Dietrich, A., Stolz, W., 2000a. The basic principle of radioluminescence dating and a localized transition model. *Radiation Measurements* 32, 487–492. doi: 10.1016/S1350-4487(00)00119-0.
- Trautmann, T., Krbetschek, M.R., Dietrich, A., Stolz, W., 1999a. Feldspar radioluminescence: a new dating method and its physical background. *Journal of Luminescence* 85, 45–58. https://doi:10.1016/S0022-2313(99)00152-0.
- Trautmann, T., Dietrich, A., Stolz, W., Krbetschek, M.R., 1999b. Radioluminescence Dating: A New Tool for Quaternary Geology and Archaeology. *Naturwissenschaften* 86, 441–444. doi:10.1007/s001140050649
- Trautmann, T., Krbetschek, M.R., Dietrich, A., Stolz, W., 1998. Investigations of feldspar radioluminescence: potential for a new dating technique. *Radiation Measurements* 29, 421–425. doi: 10.1016/S1350-4487(98)00012-2.

- 363 Trautmann, T., Krbetschek, M.R., Stolz, W., 2000b. A systematic study of the radioluminescence
364 properties of single feldspar grains. *Radiation Measurements* 32, 685–690. doi:
365 10.1016/S1350-4487(00)00077-9.
- 366 Tsukamoto, S., Jain, M., Murray, A., Thiel, C., Schmidt, E., Wacha, L., Dohrmann, R., Frechen,
367 M., 2012. A comparative study of the luminescence characteristics of polymineral fine grains
368 and coarse-grained K-, and Na-rich feldspars. *Radiation Measurements* 47, 903-908. [https://](https://doi.org/10.1016/j.radmeas.2012.02.017)
369 doi:10.1016/j.radmeas.2012.02.017.
- 370 Valladas, H., Valladas, G., 1982. Effet de l'irradiation alpha sur des grains de quartz. *PACT* 6,
371 171–178.
- 372 Varma, V., Biswas, R.H., Singhvi, A.K., 2013. Aspects of infrared radioluminescence dosimetry
373 in K-feldspar. *Geochronometria* 40, 266–273. doi: 10.2478/s13386-013-0125-6.
- 374 Visocekas, R., 1993. Tunneling radiative recombination in K-feldspar sanidine. *Nuclear Tracks*
375 and *Radiation Measurements* 21, 175–178. doi: 10.1016/1359-0189(93)90073-I.
- 376 Wagner, G.A., Krbetschek, M.R., Degering, D., Bahain, J.J., Shao, Q., Falguères, C., Voinchet,
377 P., Dolo, J.M., Garcia, T., Rightmire, G.P., 2010. Radiometric dating of the type-site for *Homo*
378 *heidelbergensis* at Mauer, Germany. *Proceedings of the National Academy of Sciences* 107,
379 19726–19730. doi: 10.1073/pnas.1012722107.
- 380 Wallinga, J., Murray, A., Wintle, A., 2000. The single-aliquot regenerative-dose (SAR) protocol
381 applied to coarse-grain feldspar. *Radiation Measurements* 32, 529-533. doi: [10.1016/S1350-](https://doi.org/10.1016/S1350-4487(00)00091-3)
382 [4487\(00\)00091-3](https://doi.org/10.1016/S1350-4487(00)00091-3)
- 383 White, W.B., Matsumura, M., Linnehan, D.G., Furukawa, T., Chandrasekhar, B.K., 1986.
384 Absorption and luminescence of Fe³⁺ in single-crystal orthoclase. *American Mineralogist* 71,
385 1415–1419.
- 386 Wintle, A.G., 1973. Anomalous fading of thermoluminescence in mineral samples. *Nature* 245,
387 143–144. <https://doi.org/10.1038/245143a0>.

- 388 Wintle, A.G., Murray, A.S., 2006. A review of quartz optically stimulated luminescence
389 characteristics and their relevance in single-aliquot regeneration dating protocols. *Radiation*
390 *Measurements* 41, 369–391. doi: [10.1016/j.radmeas.2005.11.001](https://doi.org/10.1016/j.radmeas.2005.11.001).
- 391 Wintle, A.G., Adamiec, G., 2017. Optically stimulated luminescence signals from quartz: A
392 review. *Radiation Measurements* 98, 10–33. doi:10.1016/j.radmeas.2017.02.003
- 393 Wünnemann, B., Hartmann, K., Altmann, N., Hambach, U., Pachur, H.-J., Zhang, H., 2007. 22.
394 Interglacial and Glacial Fingerprints from Lake Deposits in the Gobi Desert, NW China. In:
395 Sirocko, F., Claussen, M., Goni, M.F.S., Litt, T. (Eds.), 2007. *The Climate of Past*
396 *Interglacials*. Elsevier., 323–347
- 397 Zhang, J., Li, S.-H., 2020. Review of the Post-IR IRSL Dating Protocols of K-Feldspar. *MPs* 3, 7–
398 19. doi:10.3390/mps3010007

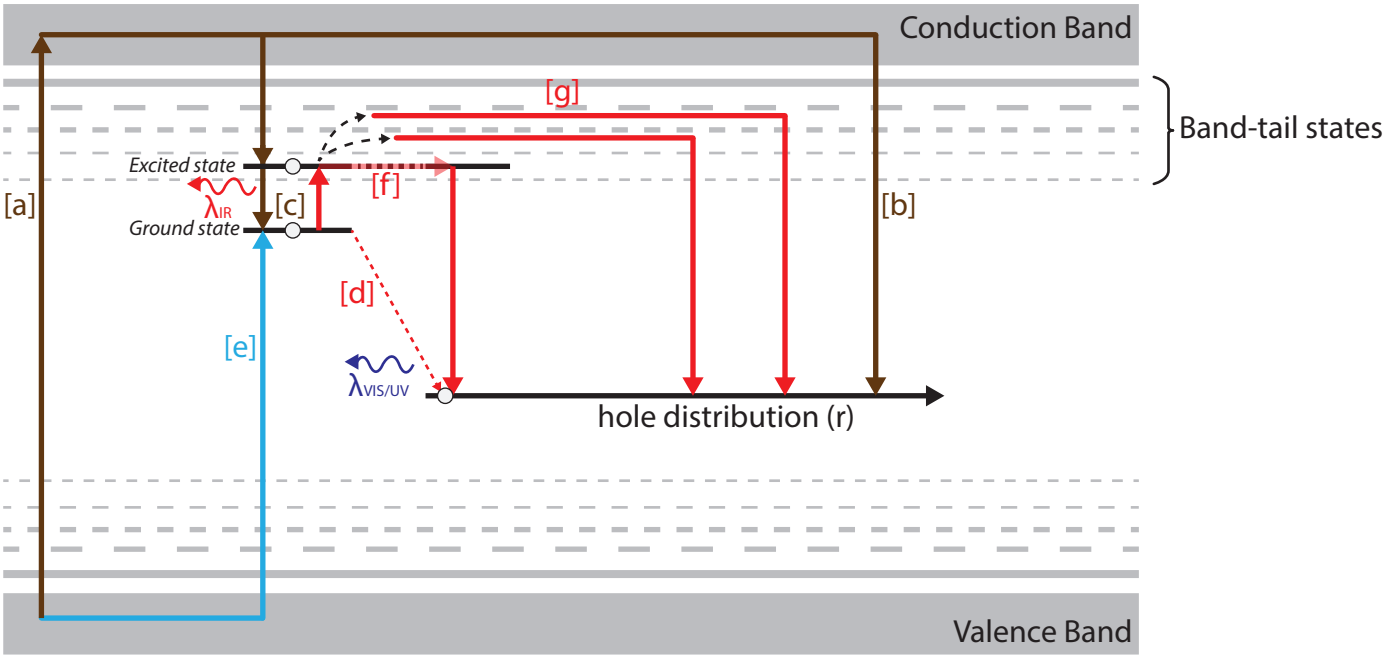
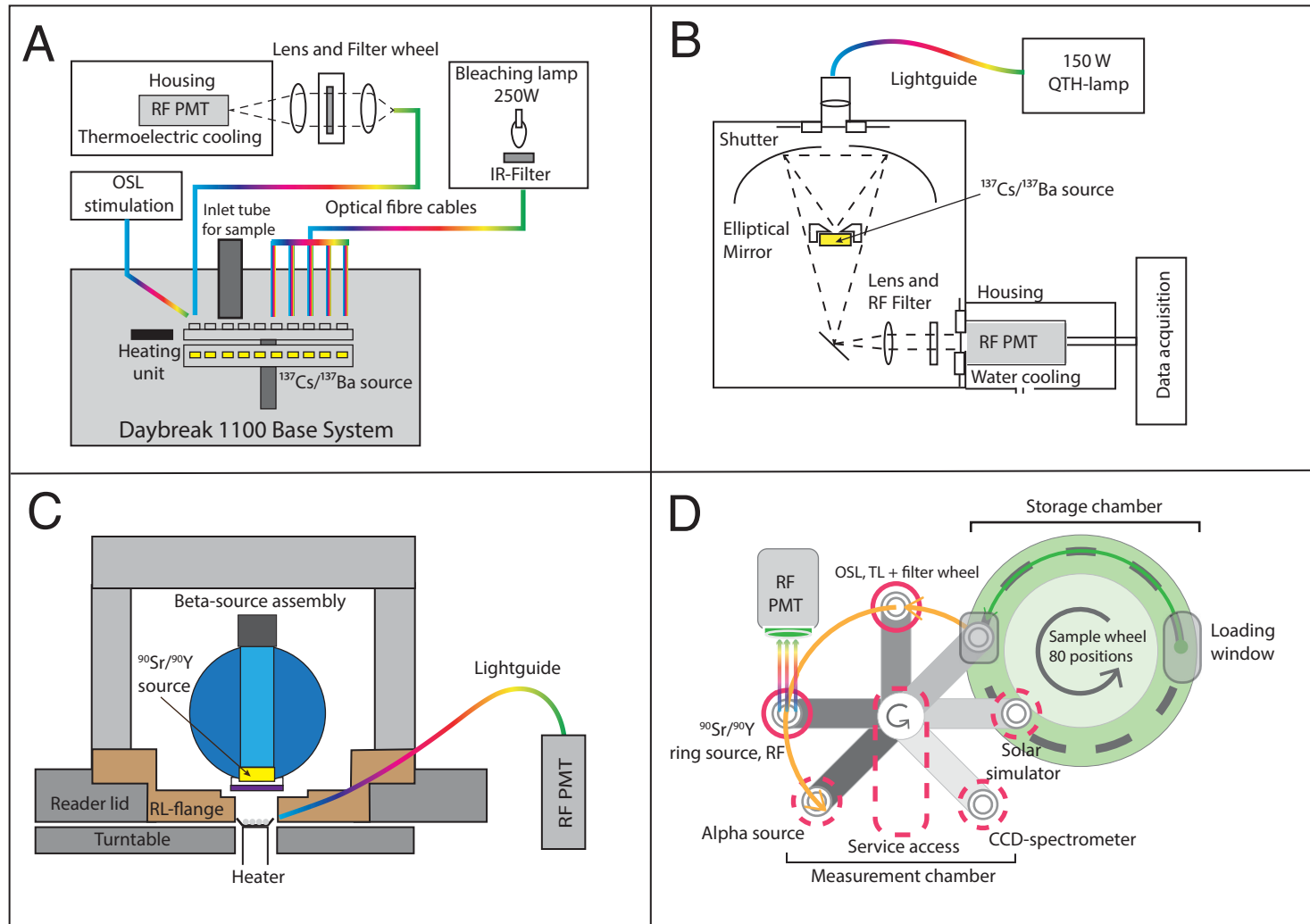
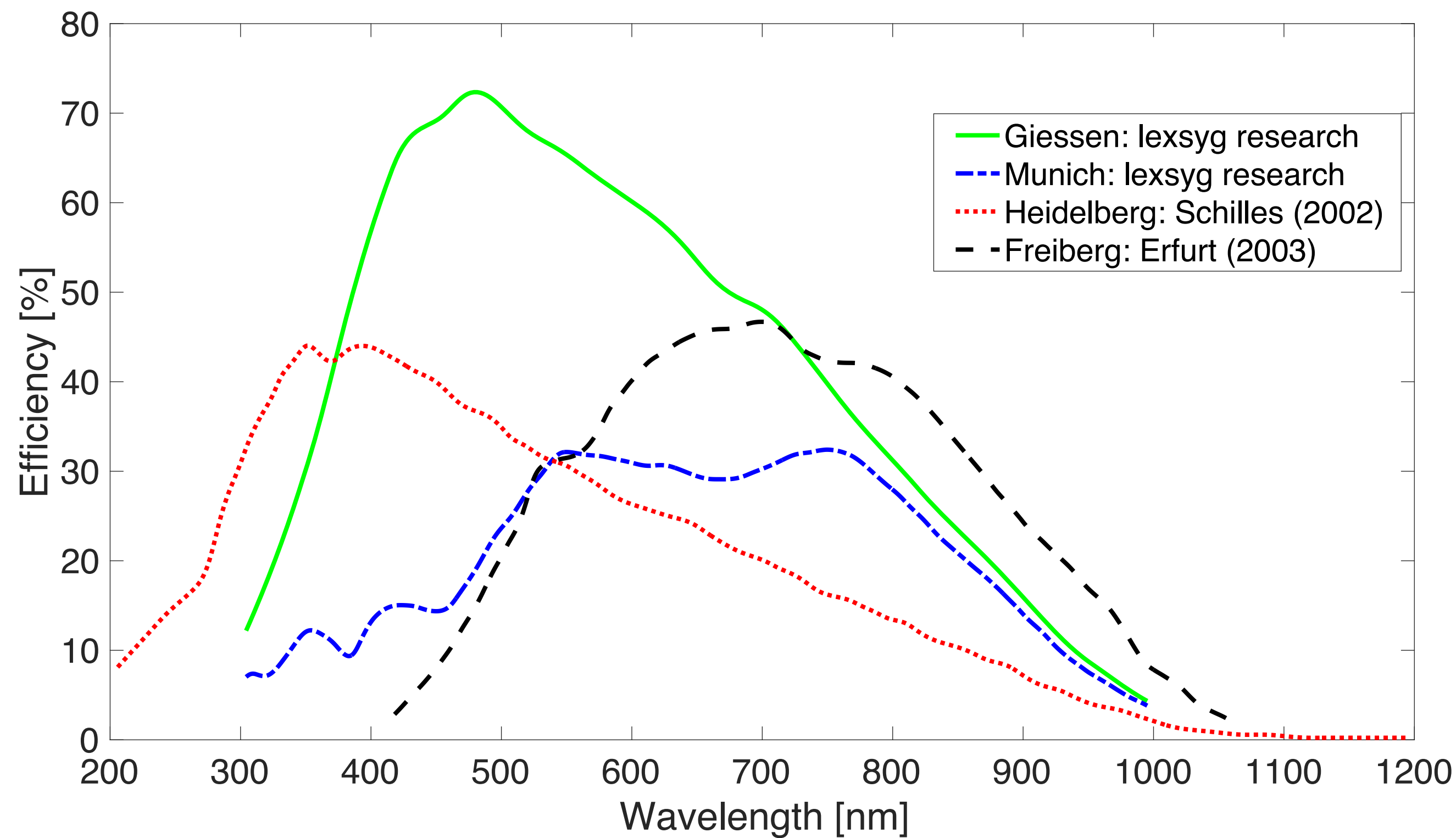


Figure 2

[Click here to access/download;Figure;Figure2_new.pdf](#)





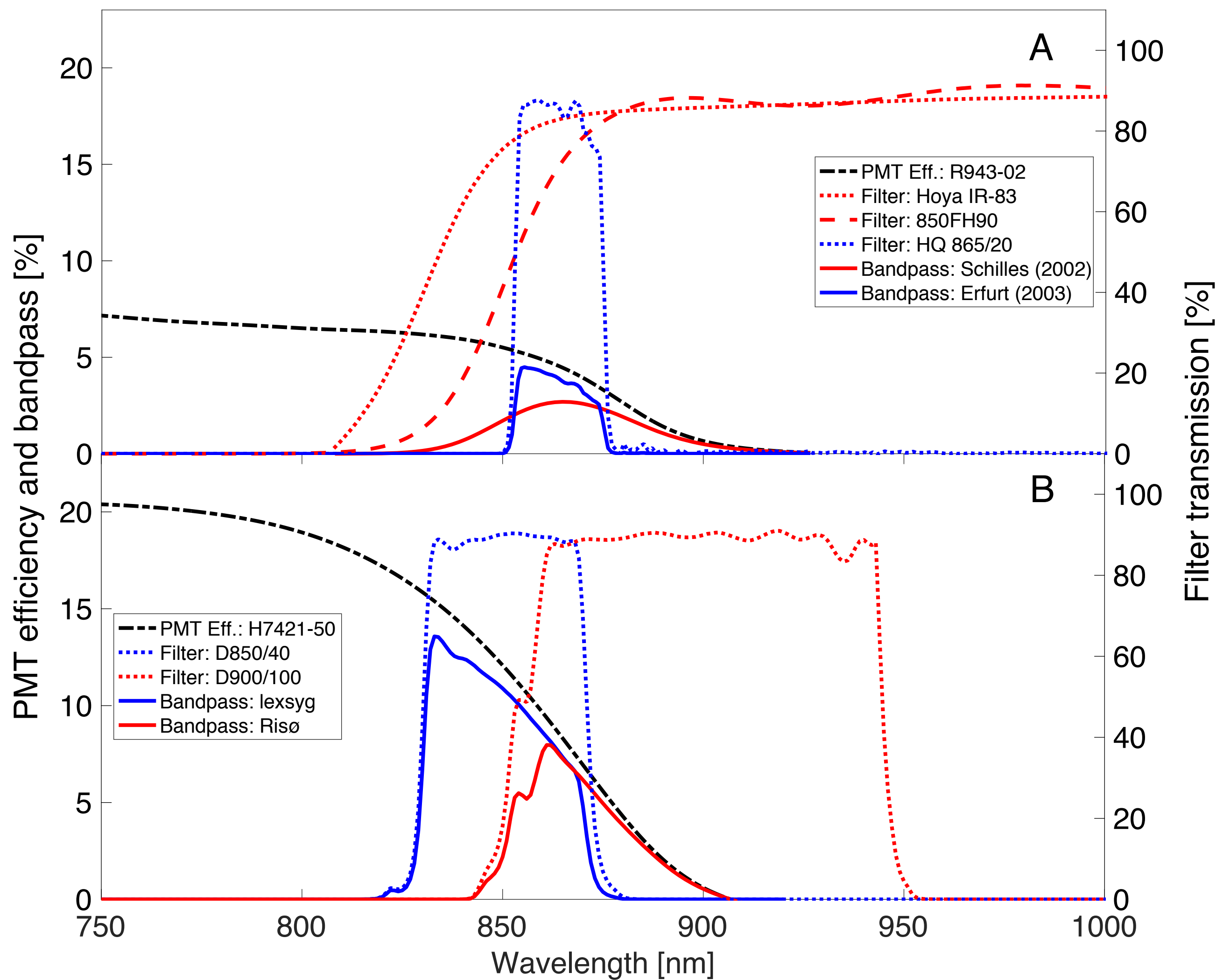
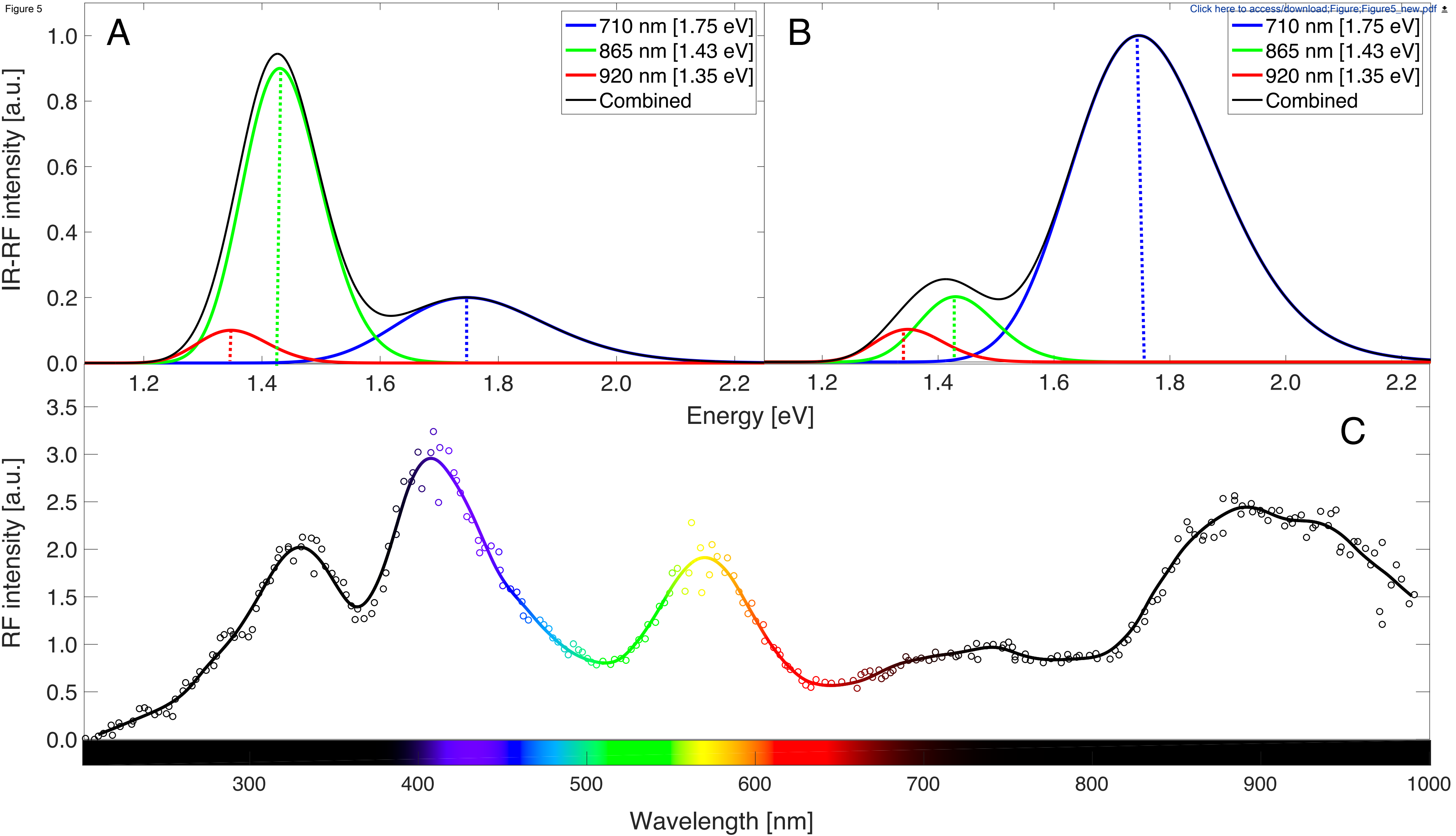


Figure 5



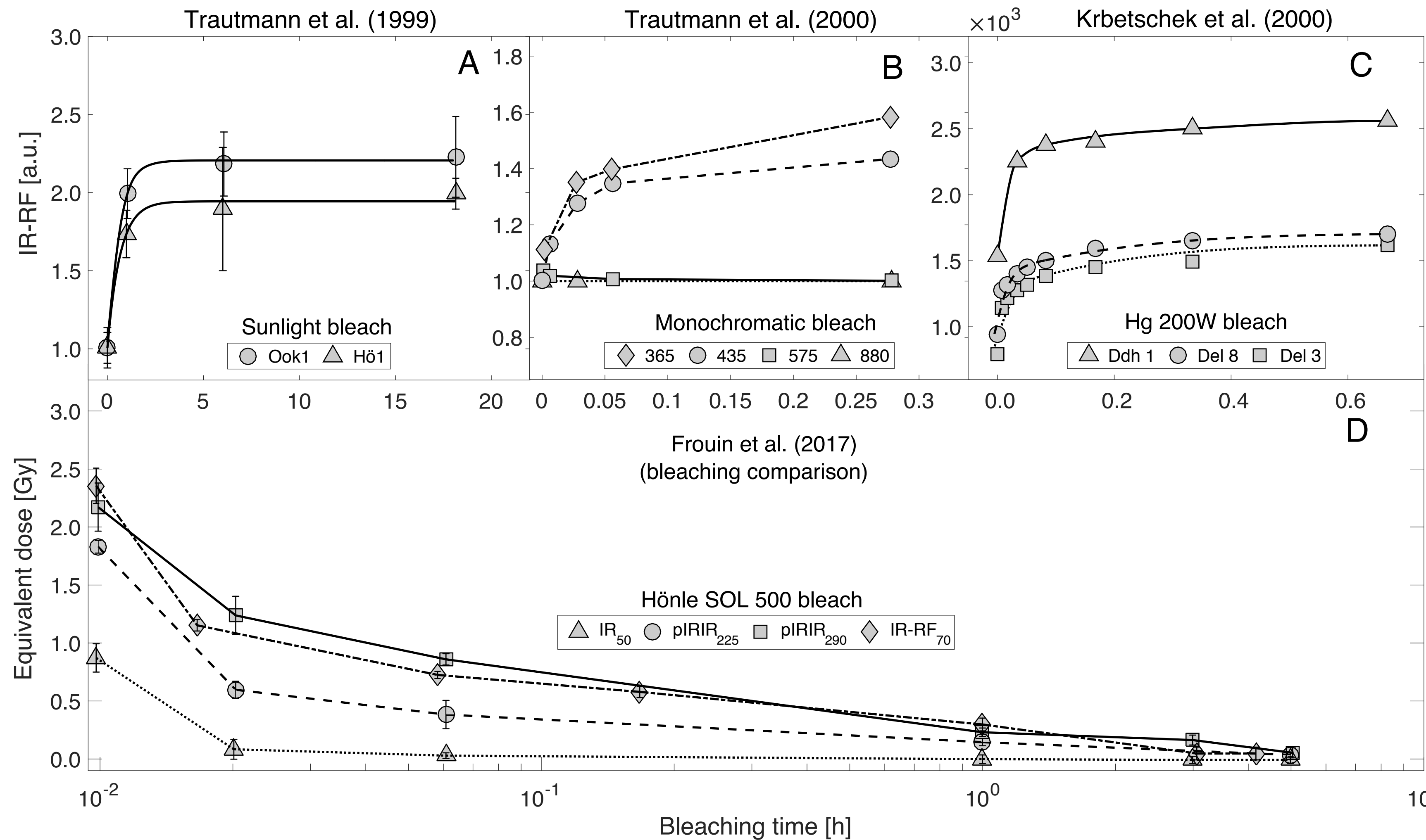


Figure 7

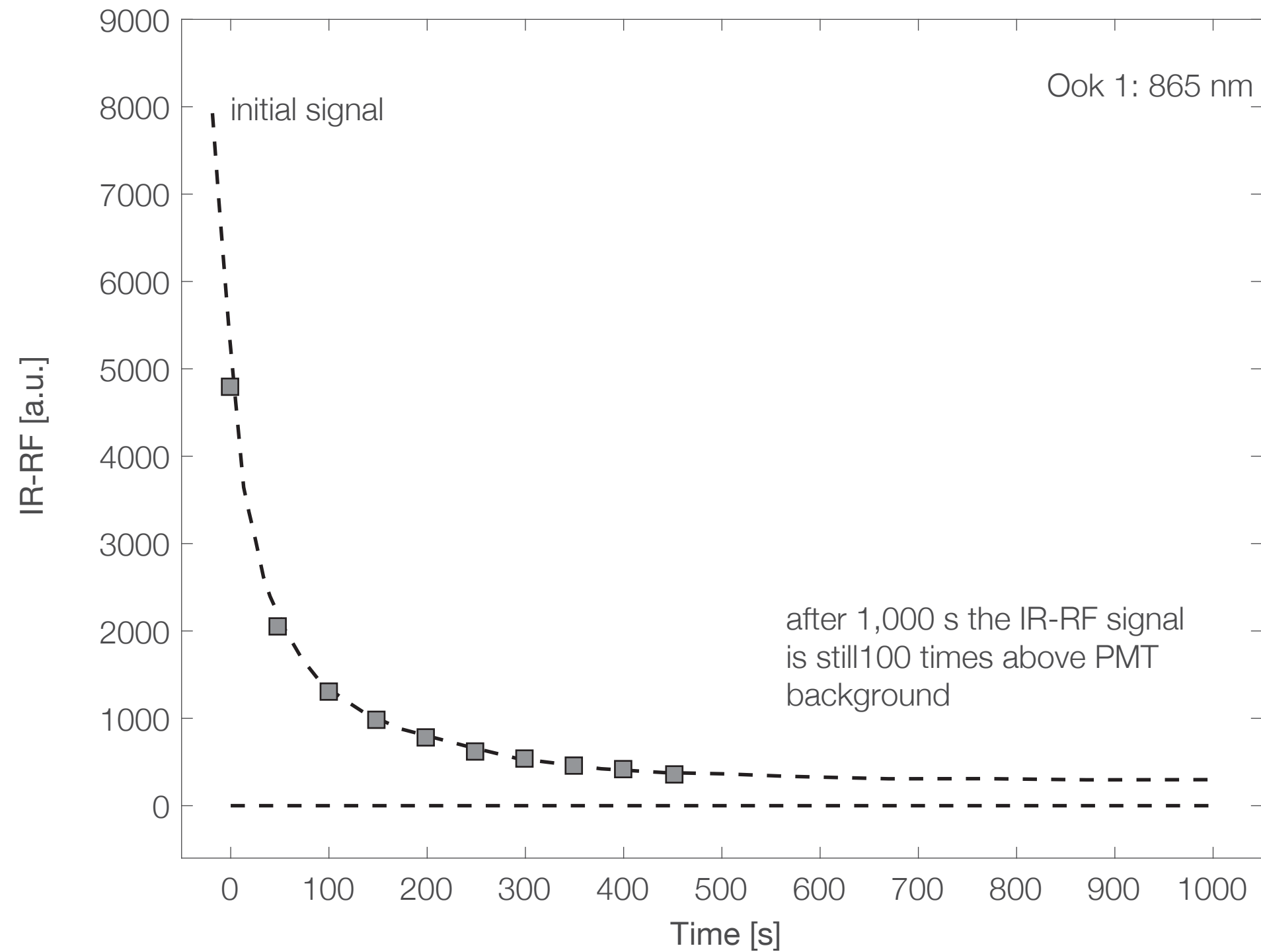


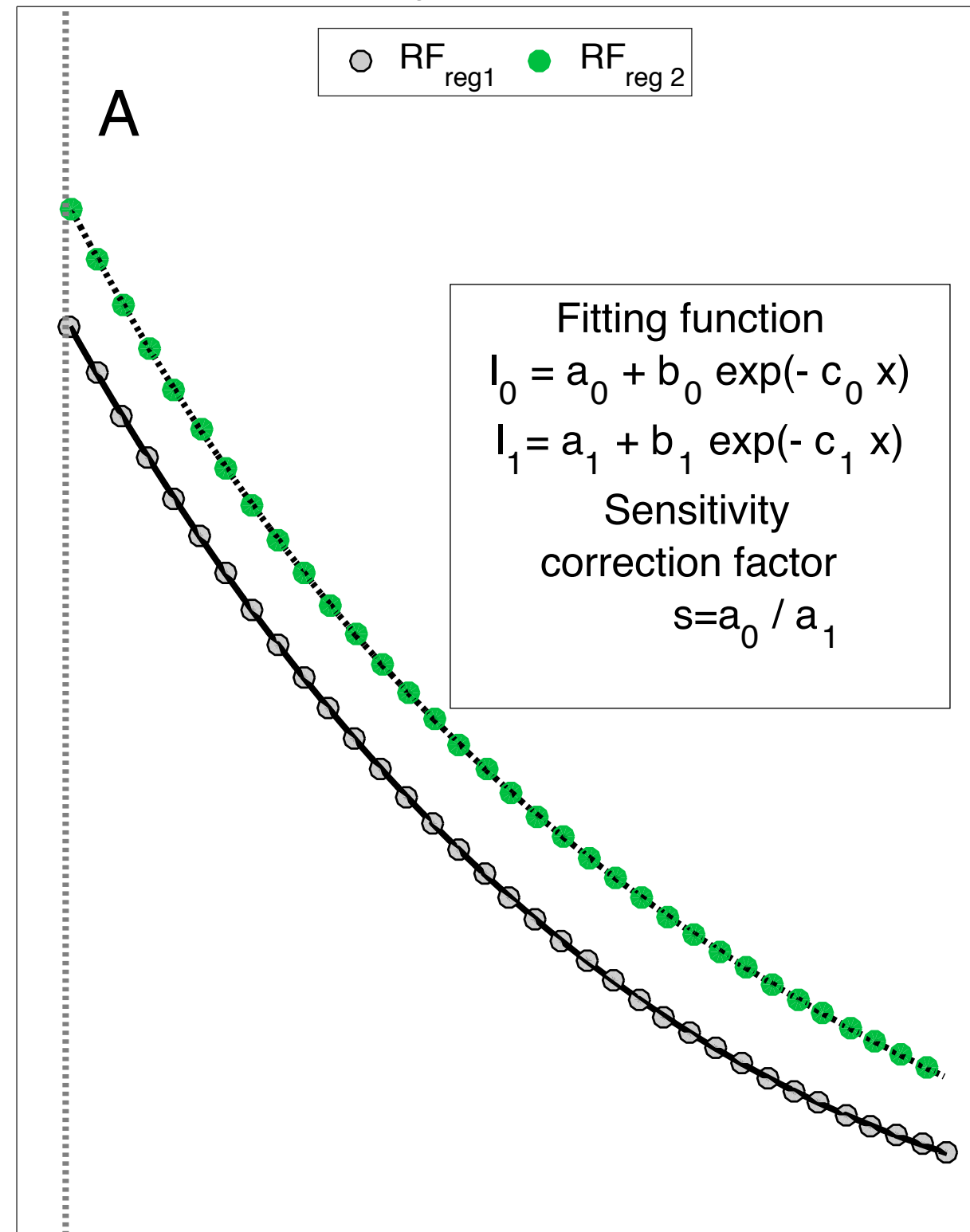
Figure 8

IR-RF [a.u.]

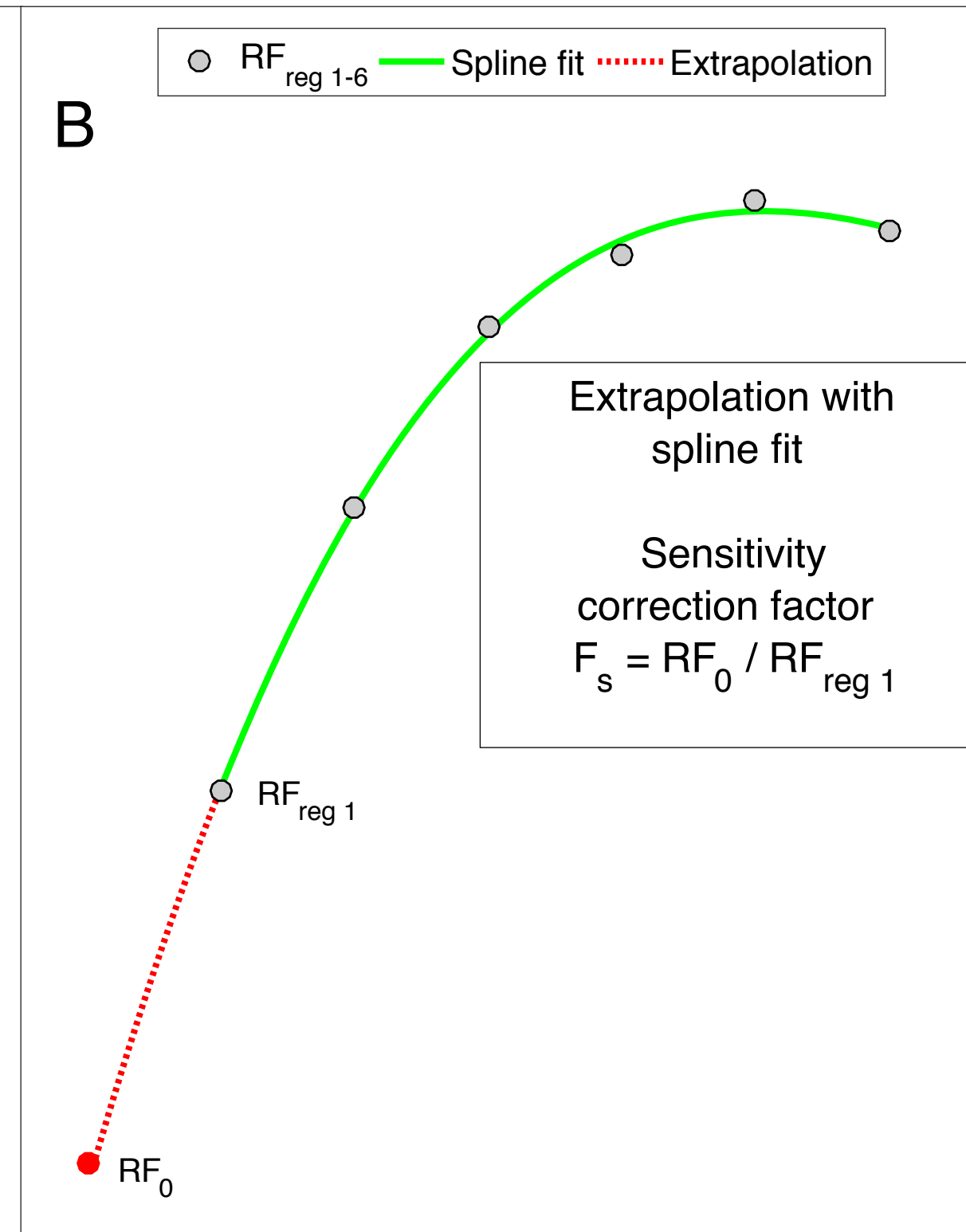
Sensitivity I Schilles (2002)

Sensitivity I Varma et al. (2013)

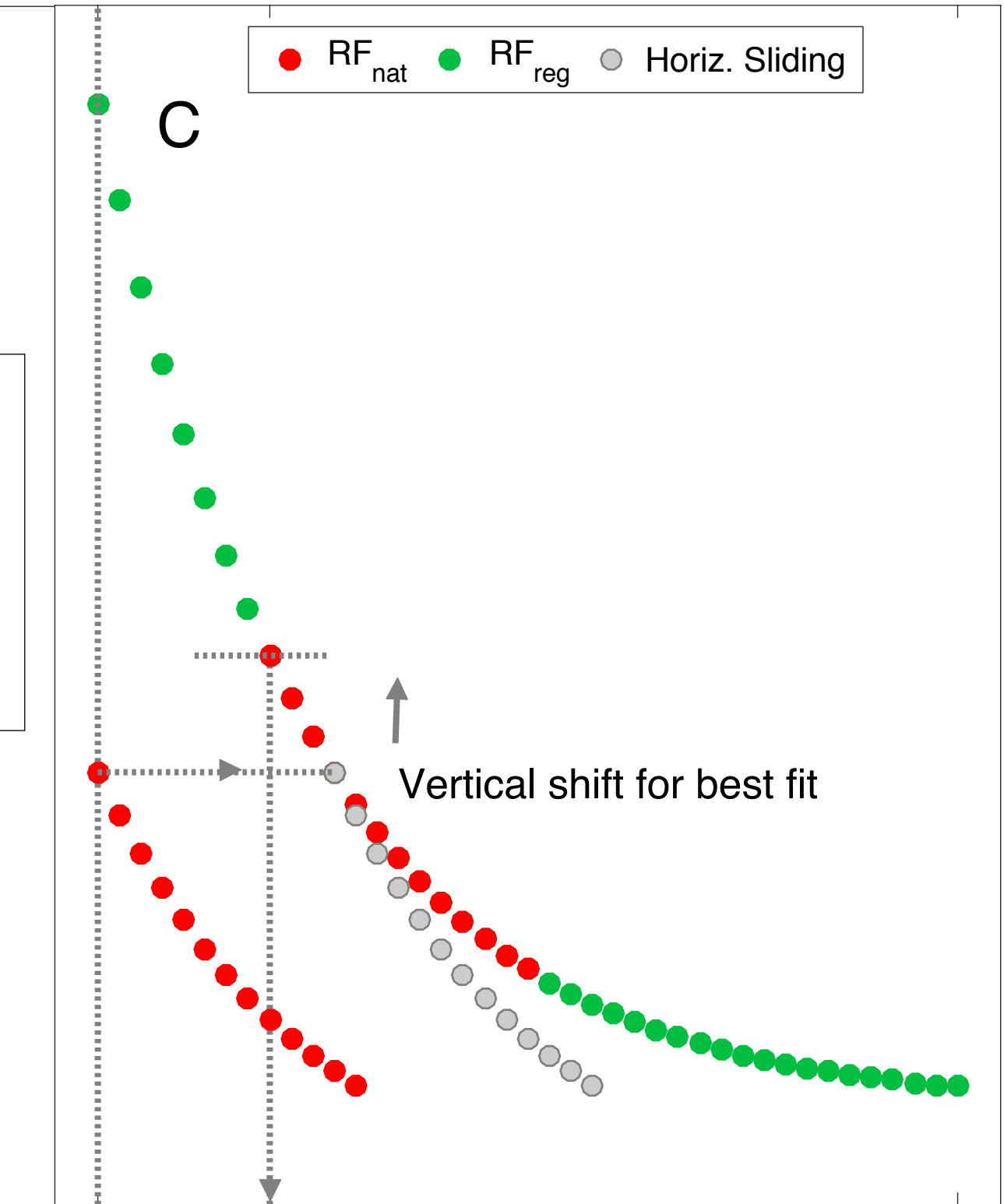
Sensitivity I Murari et al. (2018)



IR-RF Dose



Number of regenerated IR-RF cycles

 D_0 D_e

IR-RF Dose

 D_{max}

